Electronic Supplementary Information (ESI)

A coumarin-derived multi-faceted optical material with molecular logic gate for bioimaging

Amit K. Singh[a], Pranjalee Yadav[a], Aayoosh Singh[a], Avanish K. Singh[a], Shashi K. Sharma[b], Vijay K. Sonkar[b], Vinod P. Singh[a*]

[a] *Department of Chemistry, Institute of Science, Banaras Hindu University, Varanasi-221005, India.*

[b] *Department of Molecular and Human Genetics, Institute of Science, Banaras Hindu University, Varanasi-221005, India*

Table of Contents

	Experimental	S3-S8
Fig. S1	IR spectrum of **HCFH.**	**S8**
Fig. S2	^{1}H NMR spectrum of **HCFH.**	**S9**
Fig. S3	^{13}C NMR spectrum of **HCFH.**	**S9**
Fig. S4	Mass spectrum of **HCFH.**	**S10**
Fig. S5	**(a)** Hirshfeld surface analysis mapped over shape index, de, curvedness and fragment patch; **(b)** 2D fingerprint plot of **HCFH** displaying percentage of C-H, C-C, N-H, O-H, H-H, C-N O-O, C-O and N-O interactions	**S10**
Fig. S6	Absorbance spectra of **HCFH** (20 μM) at varying THF-H_2O fraction.	**S11**
Fig. S7	SEM images demonstrating aggregation with increasing water fraction: **(a)** f_w=40% and **(b)** 80%. (Scale 1 μm).	**S12**
Fig. S8	**(a)** Particle size of **HCFH** (fw=40%) measured by DLS in THF **(b)** Correlation coefficient vs time profile diagram for **HCFH** (fw=40%) in THF **(c)** Particle size of **HCFH** (fw=80%) measured by DLS in THF **(d)** Correlation coefficient vs time profile diagram for **HCFH** (fw=80%) in THF.	**S13**
Fig. S9	Fluorescence lifetime spectra of **HCFH** (20 μM) at different water fractions (f_w) **(a)** 40%, **(b)** 80%, and **(c)** 99.99% in THF.	**S14**
Fig. S10	Absorption spectra of **HCFH** (20 μM) at varying ethanol–glycerol fraction.	**S15**
Fig. S11	Absorption spectra of **HCFH** (20 μM) in the presence of various metal ions (1 equiv.) in H_2O at pH 7.4, HEPES buffer solution.	**S15**
Fig. S12	Absorption titration spectra of **HCFH** (20 μM) in H_2O (pH 7.4) HEPES buffer solution **(a)** in the presence of increasing Zn^{2+} concentration (0-2 equiv.); **(b)** in the presence of increasing Cu^{2+} concentration (0-2 equiv.).	**S16**

Fig. S13	**(a)** Fluorescence spectra and **(b)** Absorption spectra of **HCFH** after addition of Zn^{2+} with different counter anions in H_2O (pH 7.4) HEPES buffer solution. **(c)** Fluorescence spectra and **(d)** Absorption spectra of **HCFH** after addition of Cu^{2+} with different counter anions in H_2O (pH 7.4) HEPES buffer solution.	**S17**
Fig. S14	**(a)** Surface morphology of **HCFH**, **(b)** Surface morphology of **HCFH** after the interaction with Zn^{2+} and **(c)** Surface morphology of **HCFH** after the interaction with Cu^{2+} (Scale 1μm).	**S18**
Fig. S15	**(a)** Particle size of **HCFH** (20 μM) measured with DLS in water **(b)** Correlation coefficient vs time profile diagram for **HCFH** (20 μM) measured with DLS in water **(c)** Particle size of **HCFH** + Zn^{2+} (20 μM) measured with DLS in water **(d)** Correlation coefficient vs time profile diagram for **HCFH** + Zn^{2+} (20 μM) measured with DLS in water.	**S19**
Fig. S16	Limit of detection (LOD = 3σ/Slope) curve plot, the change in fluorescence intensity at 496 nm of **HCFH** (20 μM) as a function of **(a)** Zn^{2+} concentration and **(b)** Cu^{2+} concentration.	**S20**
Fig. S17	Benesi-Hildebrand plot of **HCFH** for determination of binding constant with **(a)** Zn^{2+} and **(b)** Cu^{2+}. R^2 denotes Goodness of fit. (λem = 496 nm, λex = 400 nm).	**S20**
Fig. S18	**(a)** Job's plot for determination of binding stoichiometry of **HCFH**-Zn^{2+} and **(b)** binding stoichiometry of **HCFH**-Cu^{2+}.	**S21**
Fig. S19	^1H NMR titration of **HCFH** after addition of Zn^{2+} (0-1 equiv.) in DMSO–d_6.	**S21**
Fig. S20	IR spectrum of **HCFH**-Zn^{2+} complex.	**S22**
Fig. S21	IR spectrum of **HCFH**-Cu^{2+} complex.	**S22**
Fig. S22	Mass spectrum of **HCFH**-Zn^{2+} complex.	**S23**
Fig. S23	Mass spectrum of **HCFH**-Cu^{2+} complex.	**S23**
Fig. S24	Crystal packing structure of **HCFH**-Zn^{2+} complex and its molecular assembly.	**S24**
Fig. S25	Crystal packing structure of **HCFH**-Cu^{2+} complex and its molecular assembly.	**S24**
Fig. S26	Effect of pH variation on the fluorescence intensities of **HCFH** (20 μM) in H_2O (pH 7.4) HEPES buffer solution, and after addition of Zn^{2+} and Cu^{2+} (20 μM), (λ_{em} = 496 nm, λ_{ex} = 400 nm).	**S25**
Fig. S27	Fluorescence intensity variation of **HCFH** (20 μM) in the presence of Zn^{2+} (20 μM) with addition of different metal ions (20 μM) in H_2O pH 7.4, HEPES buffer solution.	**S25**
Fig. S28	Fluorescence intensity variation of **HCFH** (20 μM) in the presence of Cu^{2+} (20 μM) with addition of different metal ions (20 μM) in H_2O, pH 7.4, HEPES buffer solution. (λ_{em} = 496 nm, λ_{ex} = 400 nm).	**S26**
Fig. S29	**(a)** Fluorescence intensity of **HCFH** (20 μM) upon subsequent addition Cu^{2+} and EDTA, **(b)** Reversible performance of **HCFH** up to four cycles (at 496 nm).	**S26**
Fig. S30	MTT assay plot showing treatment of HeLa cells with various	**S27**

	concentration of **HCFH** (10, 25, 50, 75, 100 and 150 μM) for 12 h.	
Table S1	Crystallographic data for **HCFH**, **HCFH**-Zn^{2+} and **HCFH**-Cu^{2+}.	**S28**
Table S2	Bond Lengths for **HCFH**.	**S29**
Table S3	Bond Angles for **HCFH**.	**S29**
Table S4	Fluorescence decay parameters and quantum yields of **HCFH** in THF-H_2O mixtures at different fraction of H_2O.	**S30**
Table S5	Fluorescence decay parameters and quantum yields of **HCFH** before and after treatment with Zn^{2+}/Cu^{2+} in H_2O (pH 7.4), HEPES buffer solution.	**S30**
Table S6	Major Bond Lengths and Bond Angle for **HCFH**-Zn^{2+}.	**S31**
Table S7	Major Bond Lengths and Bond Angle for **HCFH**-Cu^{2+}.	**S31**
Table S8	Comparison of **HCFH** with other previously reported sensors.	**S32**
	References	**S32-33**

Experimental

Reagents

All the chemicals and reagents were purchased by commercial sources and utilized without further purification. The solvents and metal salts were purchased from Merck Chemicals, India. Furan-2-carbohydrazide, ethyl 3-oxobutanoate, piperidine and 2, 4-dihydroxybenzaldehyde were purchased from Sigma-Aldrich Chemicals, USA. All the investigations were carried out using Millipore water. One of the reactants 3-acetyl-7-hydroxy-2H-chromen-2-one was synthesized by a reported procedure.[1]

Physico-chemical measurements

KBr pellets were used to record FT-IR spectra in 4000-400 cm^{-1} region on a FT-IR 4700 JASCO spectrophotometer. The JEOL Resonance Inc. multinuclear FT NMR spectrometer (Model-ECZ 500R) was used to obtain ^1H and ^{13}C NMR spectra in DMSO-d_6. The chemical shifts are given in parts per million (ppm) with respect to an internal standard of tetramethylsilane (TMS). ESI-mass spectra were recorded on an HRMS SCIEX X-500R QTOF spectrometer. The Shimadzu UV-1800 spectrophotometer was used to record all the UV-Visible spectra.

Fluorescence spectra were obtained using a HORIBA FL3C-21_1959C-2118-FL fluorescence spectrophotometer. The LMPH-10 pH meter was used to monitor and adjust the pH of various solutions. The EVO-(Scanning Electron Microscope) MA15 / 18 was used to capture the SEM images. DLS measurements were conducted on a Zetasizer Ultra (ZSU5700) Malvern Panalytical (UK) Particle Size Analyzer using 633 nm laser. A Bruker D8 Advance powder X-ray diffractometer equipped with Cu Kα radiation with a Lyne Eye detector was used for the powder X-ray diffraction experiments. XtaLAB S5 Synergy-I was used to acquire single-crystal X-ray diffraction data. Solid state fluorescence was recorded on Fluorolog FL-3C-21 UV-Vis-NIR-Spectrofluorometer with an integrated sphere (Steady-state). Thermal property was analyzed by differential scanning calorimetry (DSC) on a Mettler Toledo Model-822e instrument in a nitrogen environment at the heating rate of 10 ^{o}C/min.

General procedures

The stock solutions of **HCFH** (1×10^{-2} M) and metal salts were prepared in DMSO and Millipore water, respectively. For various sensing experiments, a 20 μM solution of **HCFH** was prepared in H_2O (pH 7.4, HEPES buffer solution) by further diluting the stock solution. Absorption and emission titration experiments were conducted using the **HCFH** solution at a concentration of 1×10^{-2} M with increasing concentration of metal ion solutions (1×10^{-3} M). All the titration studies were carried out at room temperature. Nitrate salts were used for different cations, while acetate and chloride salts of Zn^{2+} and Cu^{2+} were employed to evaluate the effect of counter anions. For fluorescence studies, an excitation wavelength of 400 nm and a slit width of 2 nm were optimized.

Computational details

Theoretical investigation for **HCFH**, **HCFH**-Zn^{2+}, and **HCFH**-Cu^{2+} complexes were carried out using Gaussian 09 software with the 6-311G (d, p) basis set and the RB3LYP method. The minima of the potential energy of the DFT optimized structures were confirmed to validate the results.[2]

X-ray crystallography

The Rigaku XtaLAB Synergy-I diffractometer with CrysAlisPro was used to conduct the single crystal X-ray diffraction studies with a graphite monochromated Mo Kα (λ = 0.71073 Å) and Cu Kα (λ = 1.54184 Å) radiation sources were used to get the single crystal X-ray diffraction data at 293 K and 100 K. The structure was solved using the SHELXL-97 program and was refined by full-matrix least-squares on F^2 with anisotropic displacement parameters applied to all non-hydrogen atoms.[3] Hydrogen atoms were refined with use of a riding model, placing them in geometrically idealized positions. Structural representations were obtained using MERCURY software and the ORTEP-3 tool for Windows.[4]

Cell culture

HeLa, cervical carcinoma cells were cultured in either T-flasks or 6- or 96-well plates, depending on the experimental design. The cells were maintained in Dulbecco's Modified Eagle Medium (DMEM) containing L-glutamine supplemented with 10% fetal bovine serum (FBS), 100 U/mL penicillin, and 100 μg/mL streptomycin to ensure optimal growth conditions. Cultures were incubated at 37°C in a CO_2 incubator, providing a controlled environment of 95% humidified air and 5% CO_2.

Cytotoxicity assay

A total of 5,000 cells were seeded into a 96-well plate and incubated in a CO_2 incubator for 24 h to allow cell attachment and growth. To assess the cytotoxicity of the **HCFH** probe, cells were exposed to varying concentrations of **HCFH** (10 to 150 μM) and incubated for 12 h in CO_2 incubator. Cell viability was evaluated using the MTT assay (3-(4,5-dimethylthiazol-2-yl)-2,5-diphenyltetrazolium bromide), as previously described.

Bio-imaging and probe localization study

To assess the fluorescence properties of the **HCFH** probe, 5,000 HeLa cells were seeded onto coverslips placed into a six-well plate and incubated for 24 h. The cells were then treated with the **HCFH** probe (20 μM) alone, or in combination with Zn^{2+} and Cu^{2+} for 1 h. After treatment, cells were fixed with 4% paraformaldehyde for 15 min, permeabilized with 0.1% Triton X-100 for 15 min, and counterstained with 10 μM DAPI for 5 min. The samples were then mounted on slides using the DABCO anti-fading agent. For the localization study of the **HCFH** probe, cells were grown and treated as described above. After 24 h incubation, cells were exposed to the **HCFH** probe (20 μM) and also incubate with 100 nM MitoTracker CMXRos simultaneously for 1 h at 37°C in a CO_2 incubator. After treatment, cells were washed, fixed, permeabilized and counterstained with DAPI. The slides were mounted for visualization using a confocal fluorescence microscope (ZEISS Imager.Z2m).

Fluorescence quantum yield measurements

Quantum yield was calculated by using the following equation:

$$Q = Q_r\left(\frac{I}{I_r}\right)\left(\frac{OD_r}{OD}\right)\left(\frac{n^2}{n_r^2}\right) \quad \dots \textbf{(1)}$$

Where Q is the fluorescence quantum yield, I is the integrated fluorescence intensity, n is the refractive index of liquid, and OD is the optical density (absorption). The subscript r is used to represent the known quantum yield of reference quinine sulphate, which is 0.54 in 0.1 M H_2SO_4.[5]

Fluorescence decay measurements

Time-resolved fluorescence spectra were recorded to explore AIE and sensing properties at the concentrations of 20 μM, respectively.

Dynamic parameters are determined from the following equation:

$$y = A_1 * \exp\left(-\frac{x}{\tau_1}\right) + A_2 * exp\left(-\frac{x}{\tau_2}\right) + y_0 \quad \ldots \textbf{(2)}$$

Weighted mean lifetime <τ> was calculated by using the following equation:

$$<\tau> = (A_1\tau_1 + A_2\tau_2)/(A_1 + A_2) \quad \ldots \textbf{(3)}$$

Where, A_1/A_2 and τ_1/τ_2 are the fractions or amplitudes (A) and lifetimes (τ), respectively.
The radiative rate constant (K_r) and non-radiative rate constant (K_{nr}) are calculated from the following equations:[6]

$$<\tau^{-1}> = (K_r + K_{nr}) \quad \ldots \textbf{(4)}$$

$$K_r = \frac{\Phi}{<\tau>} \quad \ldots \textbf{(5)}$$

Method of calculation for detection limit (LOD)

Using fluorescence titration data, the limit of detection for HCFH was calculated by the IUPAC definition, which was based on a plot of emission intensity vs increasing Zn^{2+}/Cu^{2+} concentration. To calculate the S/N ratio, we repeated our observations eight times, each time measuring the emission intensity of HCFH without Zn^{2+}/Cu^{2+} and calculating the standard deviation of blank data. The slope was calculated by plotting fluorescence intensity data at 496 nm against Zn^{2+}/Cu^{2+} concentration. The following equation is used to establish the detection limit:

$$\text{Limit of Detection (LOD)} = \frac{3SD}{Slope(m)} \quad \ldots \textbf{(6)}$$

In this equation, m represents the slope of intensity vs sample concentration, and SD is the standard deviation of blank measurements.[7]

Method of calculation for association constant

The binding ratio of HCFH to metal ions was calculated using Job's plot and the binding constants (K_a) of HCFH for Zn^{2+} and Cu^{2+} were obtained using the Benesi-Hildebrand equation.[8]

$$\frac{I_0}{I - I_0} = \frac{a}{b - a}\left(\frac{1}{K_a[Metal]} + 1\right) \quad \ldots \textbf{(7)}$$

In this equation, I and I_0 are the intensities of HCFH fluorescence at 496 nm in the presence and absence of Zn^{2+}/Cu^{2+}, respectively; a and b are constants; and [Metal] is the concentration of Zn^{2+}/Cu^{2+}.

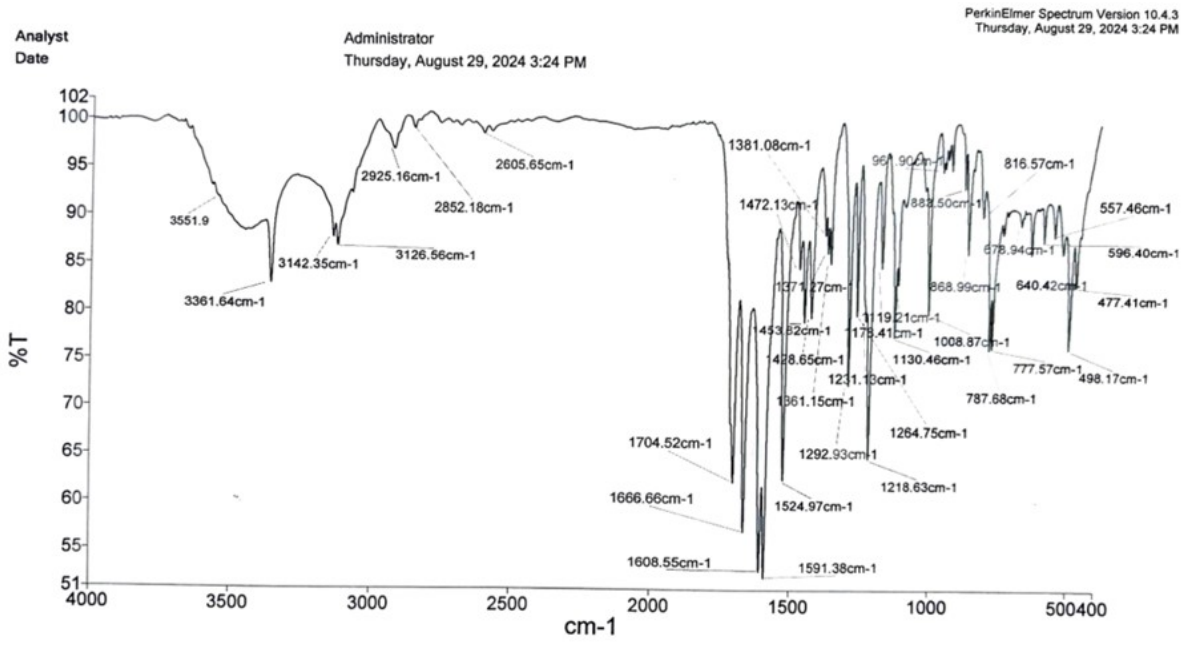

Fig. S1 IR spectrum of **HCFH**.

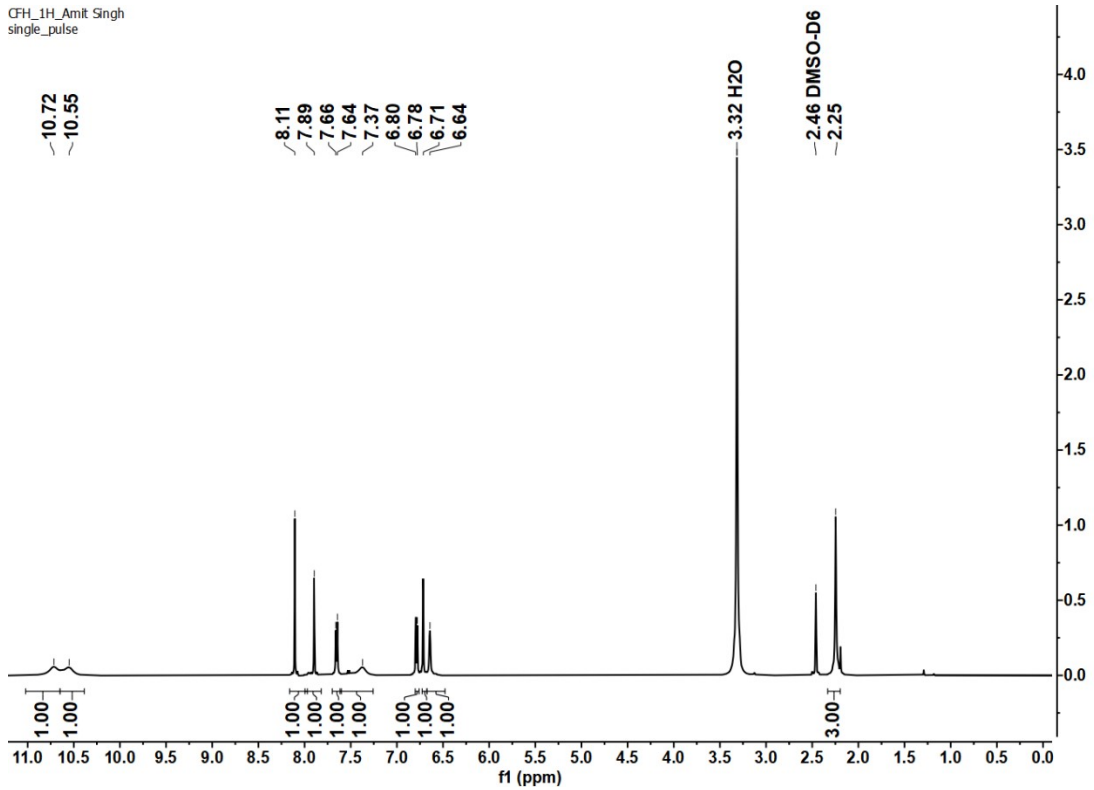

Fig. S2 ^{1}H NMR spectrum of **HCFH**.

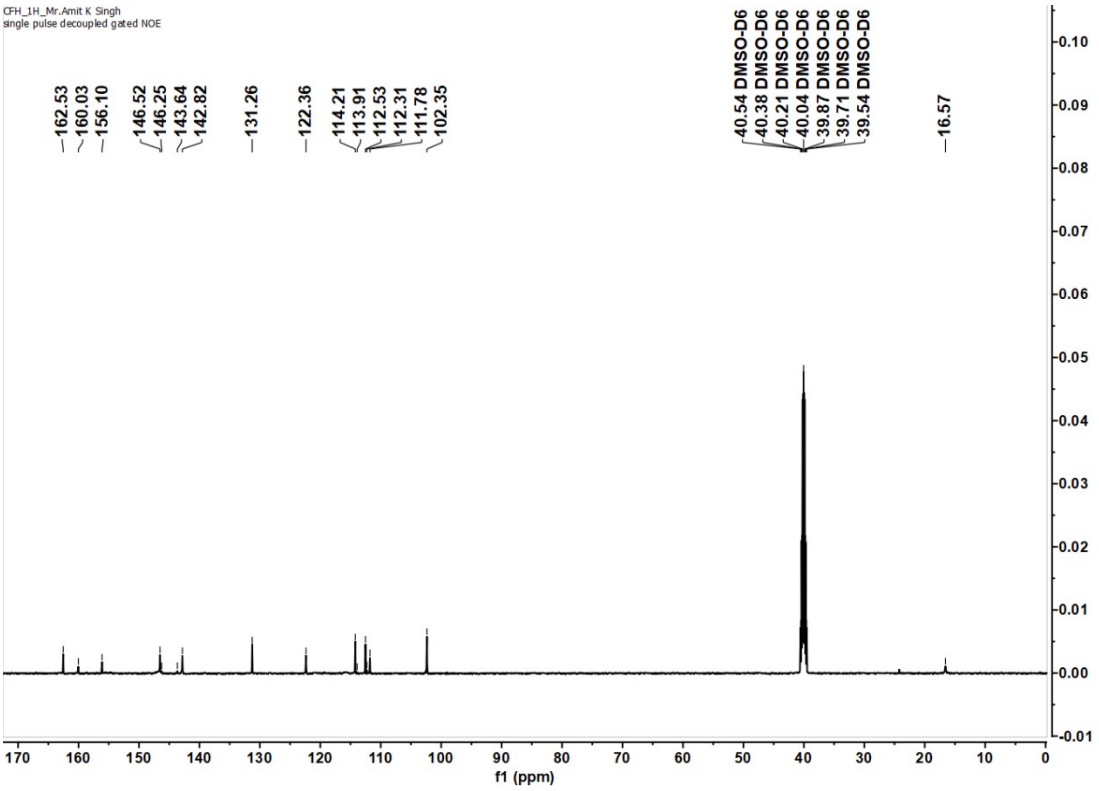

Fig. S3 ^{13}C NMR spectrum of **HCFH.**

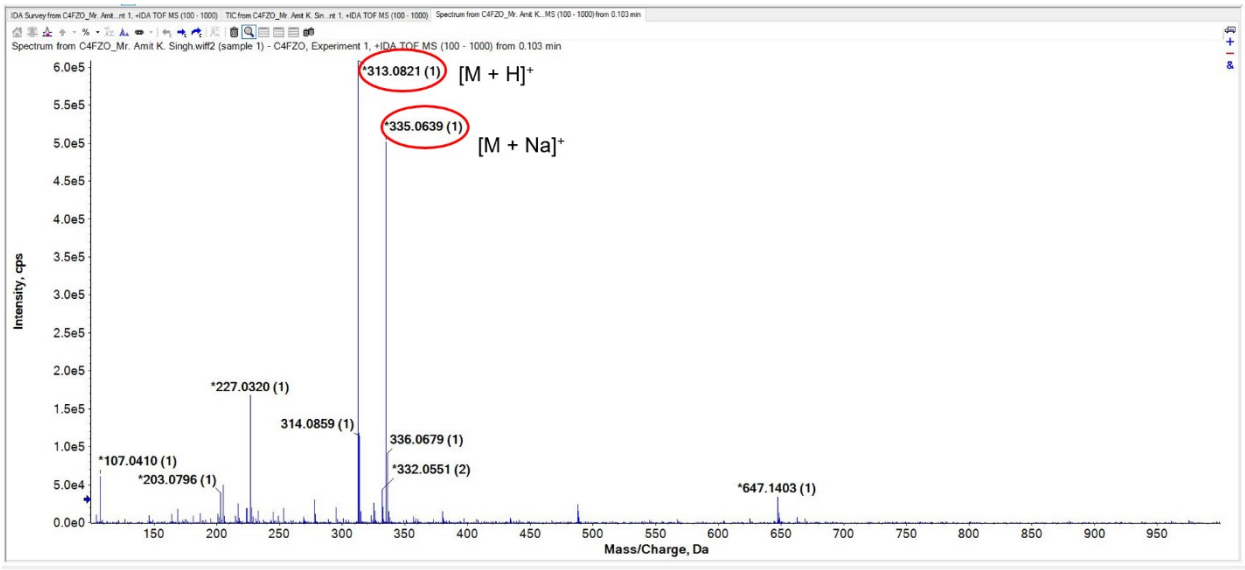

Fig. S4 Mass spectrum of **HCFH**.

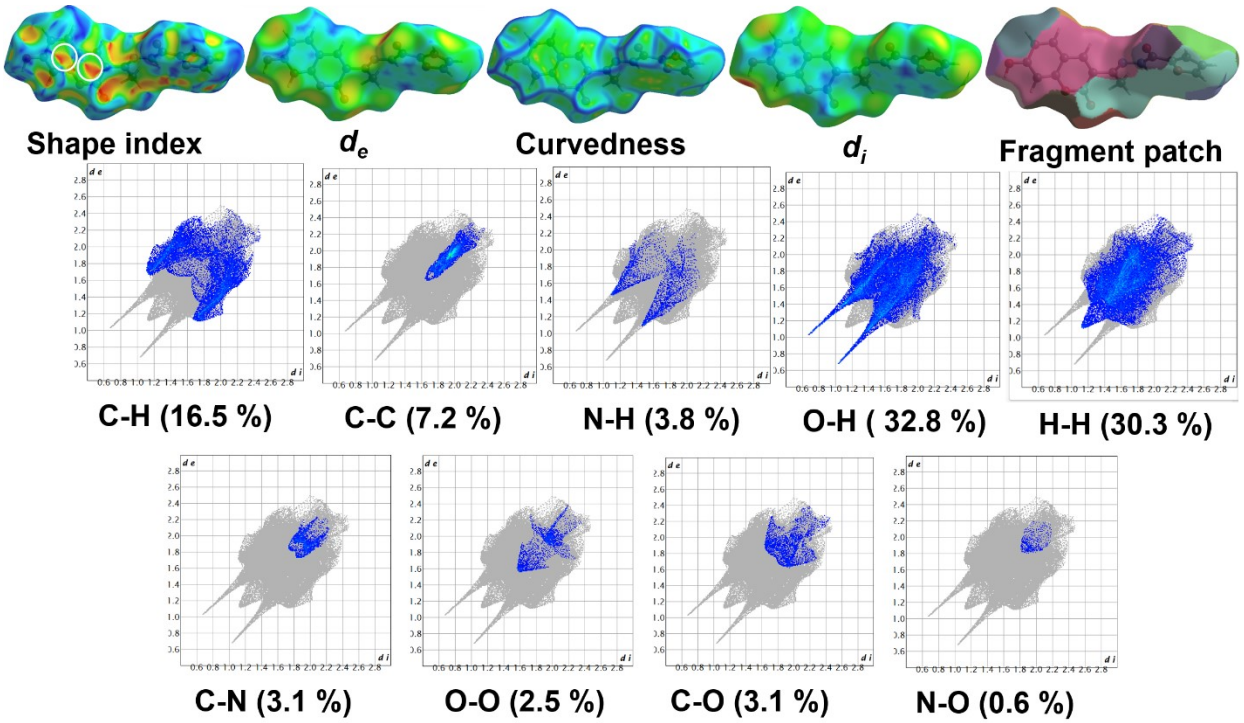

Fig. S5 (a) Hirshfeld surface analysis mapped over shape index, de, curvedness and fragment patch; **(b)** 2D fingerprint plot of **HCFH** displaying percentage of C-H, C-C, N-H, O-H, H-H, C-N O-O, C-O and N-O interactions.

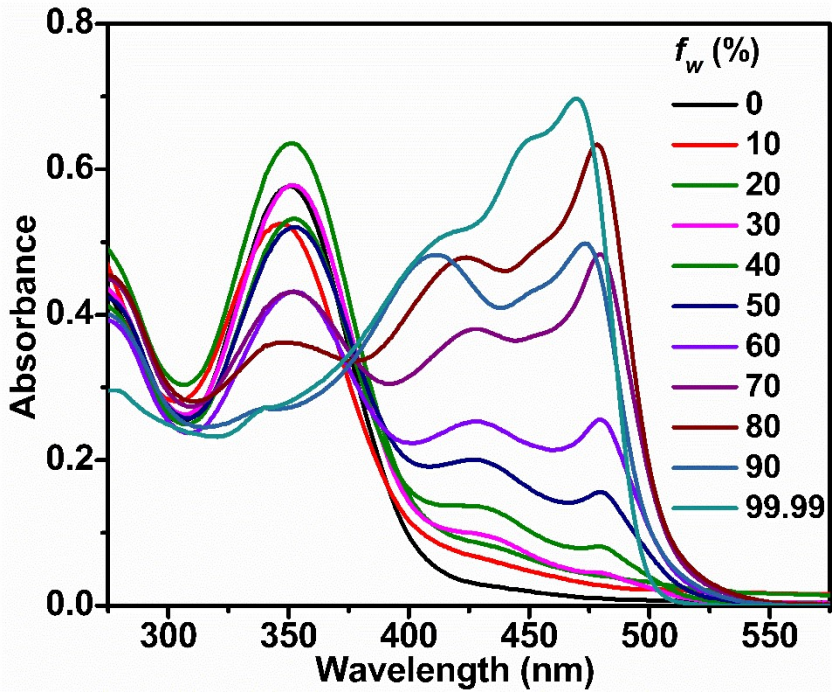

Fig. S6 Absorption spectra of **HCFH** (20 μM) at varying THF–H_2O fractions.

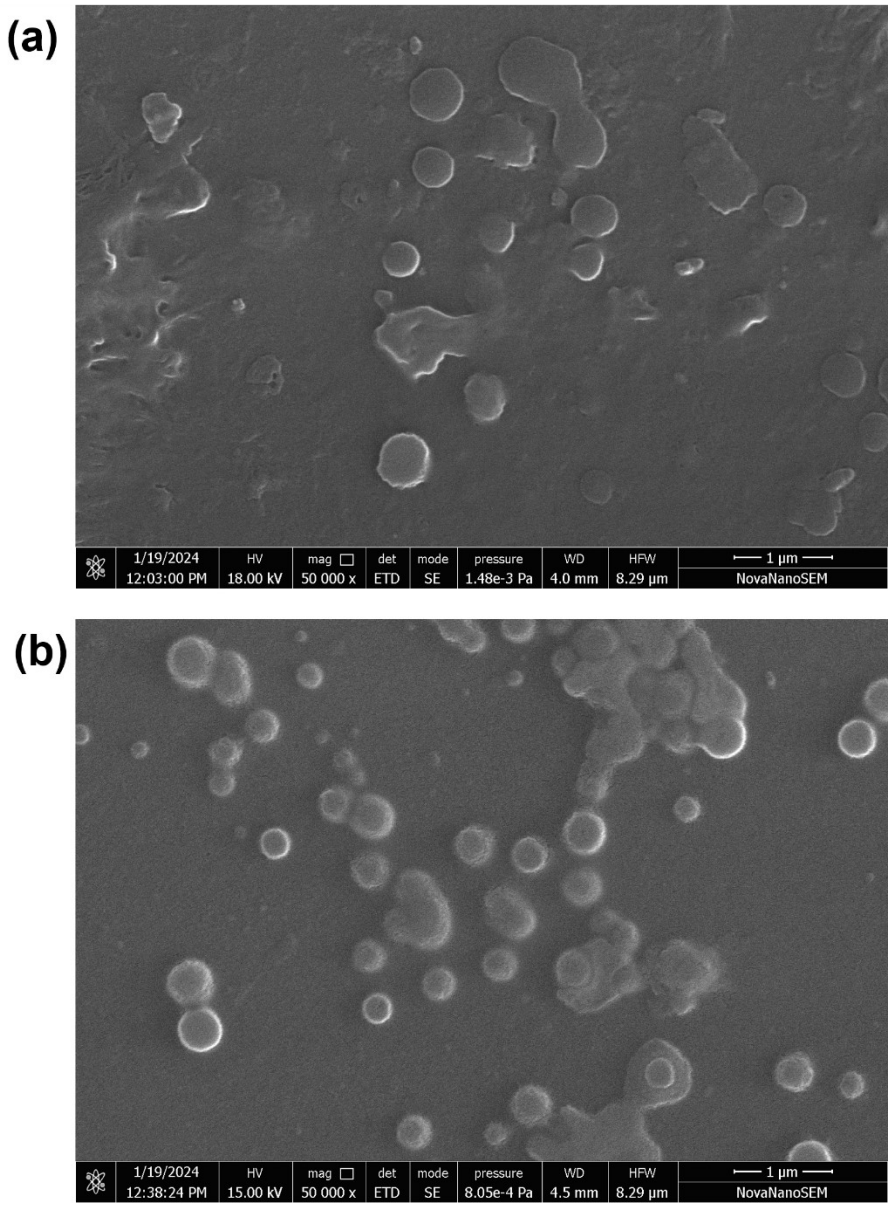

Fig. S7 SEM images demonstrating aggregation with increasing water fraction: **(a)** f_w=40% and **(b)** 80%. (Scale 1 µm).

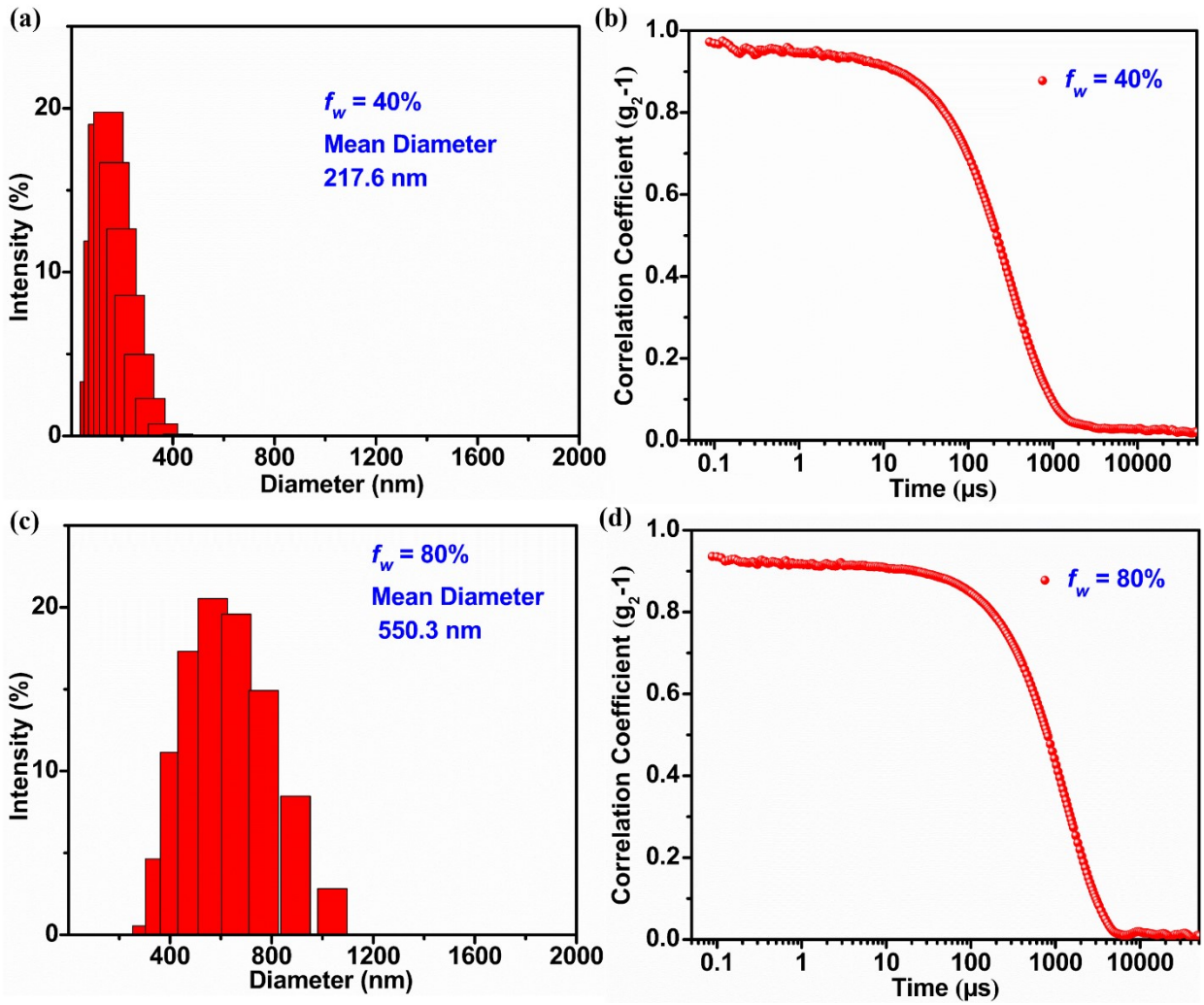

Fig. S8 (a) Particle size of **HCFH** (f_w=40%) measured by DLS in THF **(b)** Correlation coefficient vs time profile diagram for **HCFH** (f_w=40%) in THF **(c)** Particle size of **HCFH** (f_w=80%) measured by DLS in THF **(d)** Correlation coefficient vs time profile diagram for **HCFH** (f_w=80%) in THF.

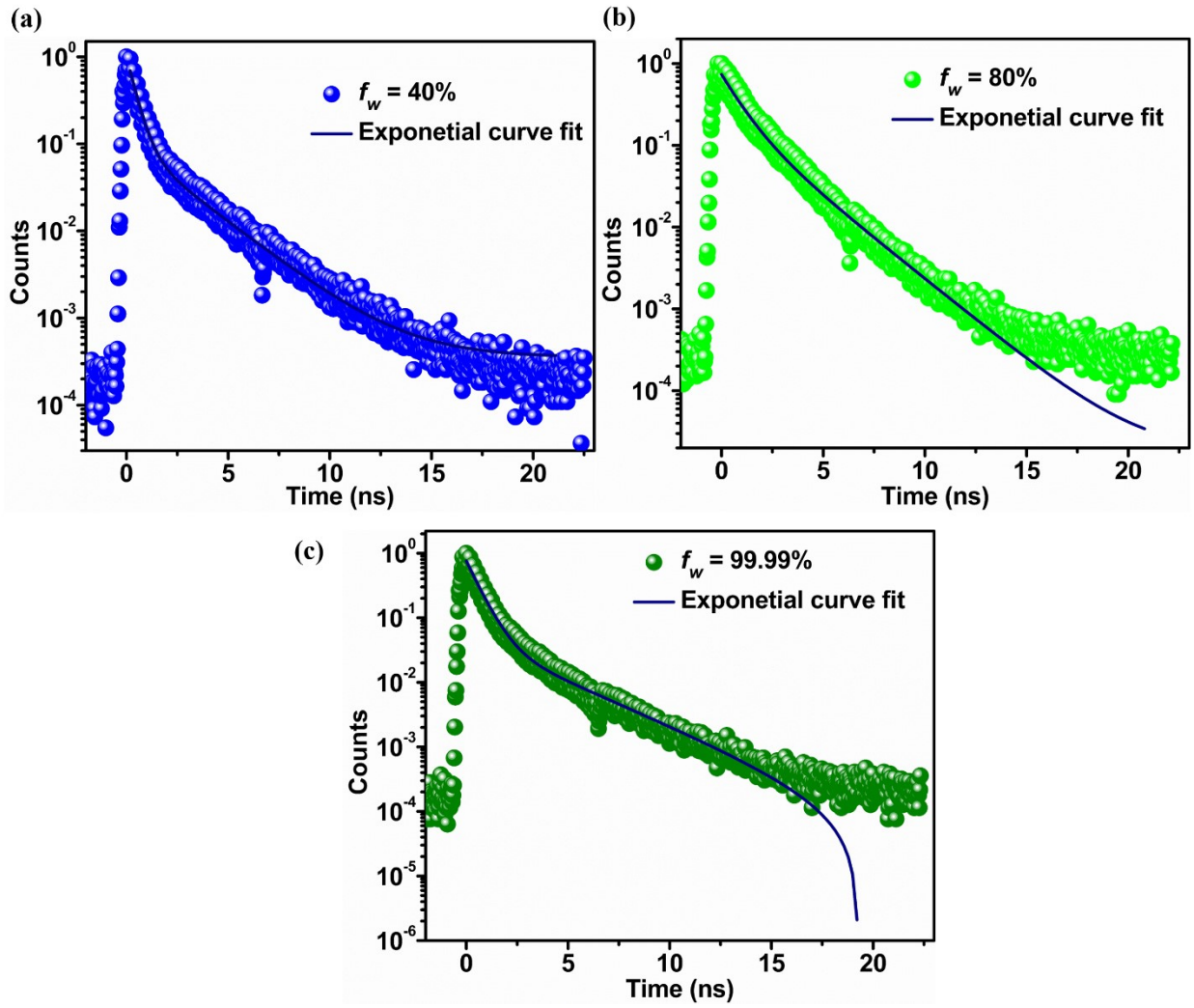

Fig. S9 Fluorescence lifetime spectra of **HCFH** (20 μM) at different water fractions (f_w) **(a)** 40%, **(b)** 80%, and **(c)** 99.99% in THF.

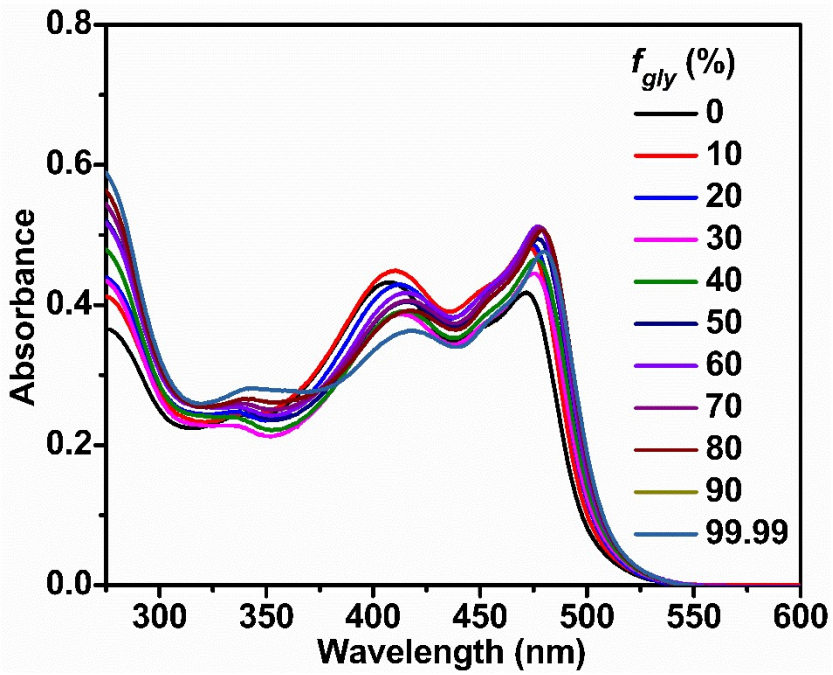

Fig. S10 Absorption spectra of **HCFH** (20 μM) at varying ethanol–glycerol fractions.

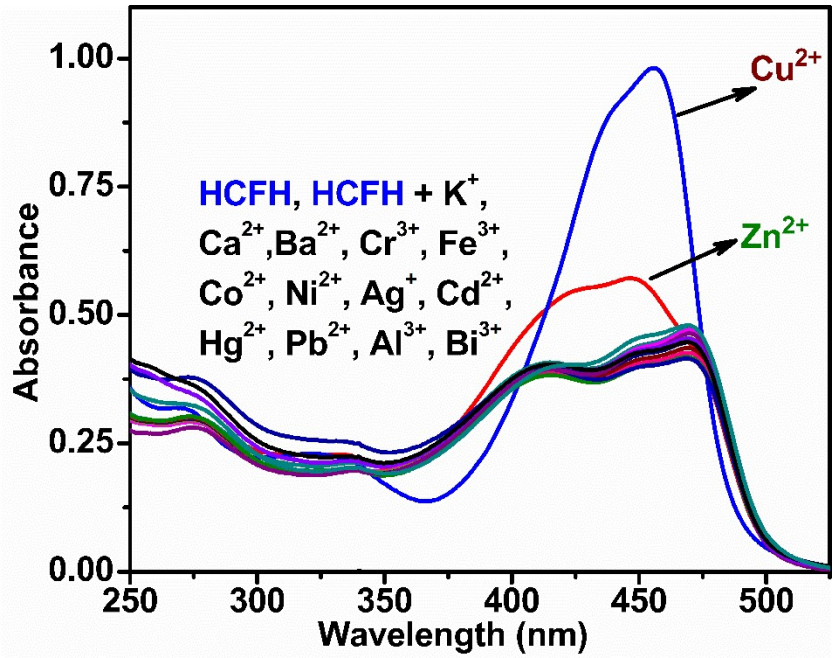

Fig. S11 Absorption spectra of **HCFH** (20 μM) in the presence of various metal ions (1 equiv.) in H_2O at pH 7.4, HEPES buffer solution.

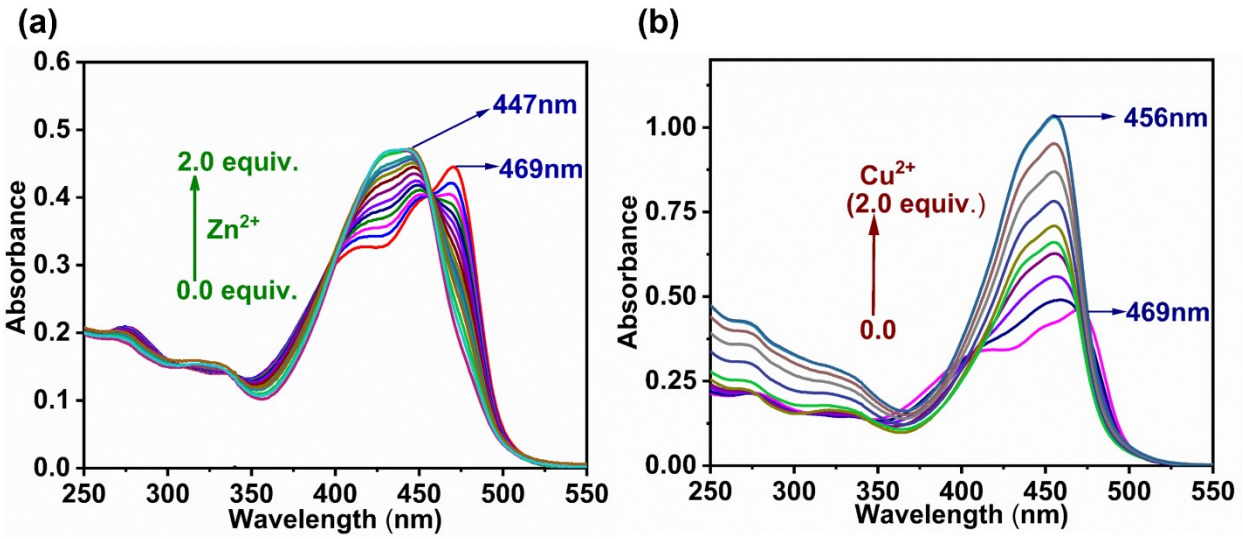

Fig. S12 Absorption titration spectra of **HCFH** (20 μM) in H_2O (pH 7.4) HEPES buffer solution **(a)** in the presence of increasing Zn^{2+} concentration (0-2 equiv.); **(b)** in the presence of increasing Cu^{2+} concentration (0-2 equiv.).

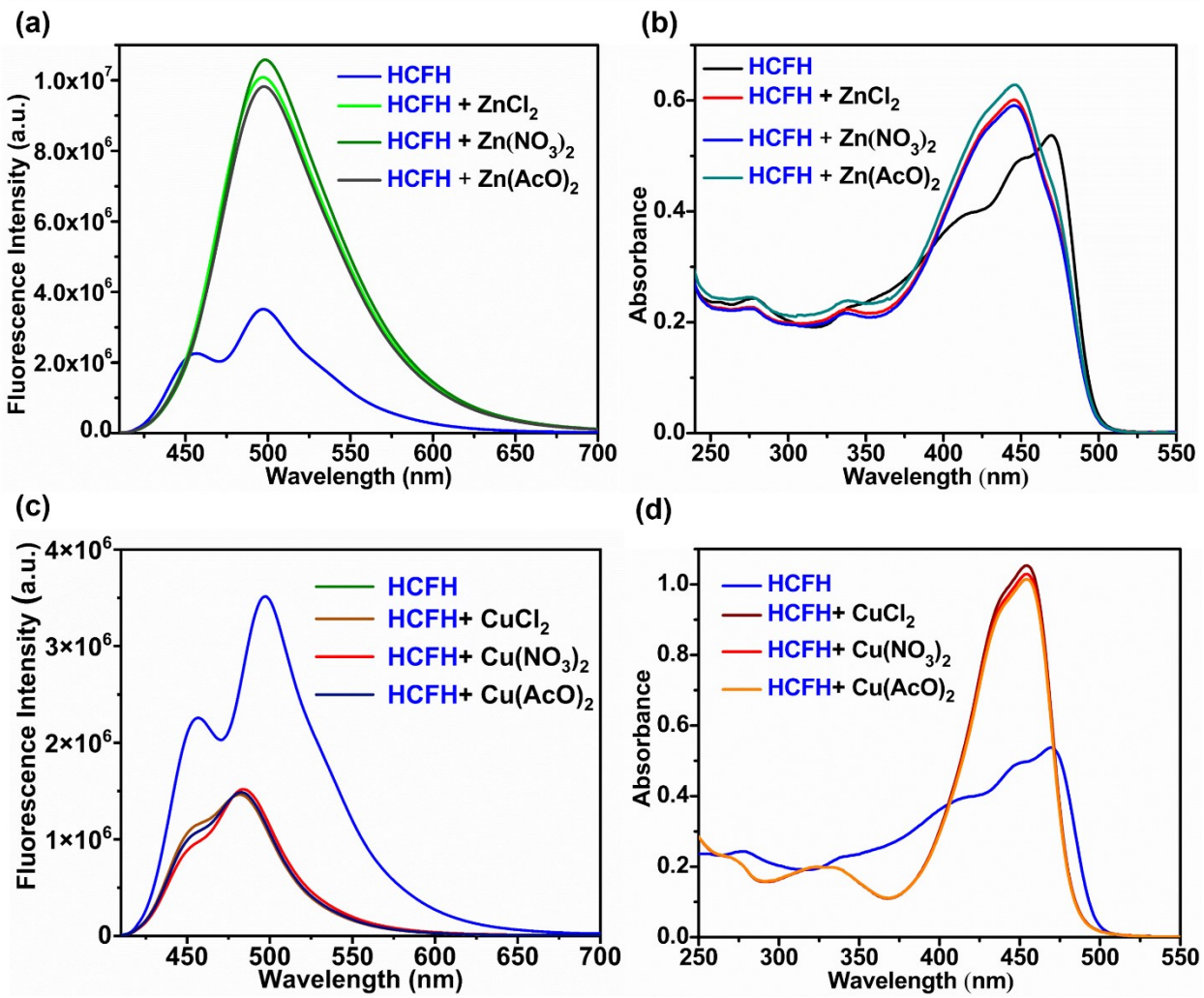

Fig. S13 (a) Fluorescence spectra and **(b)** Absorption spectra of **HCFH** after addition of Zn^{2+} with different counter anions in H_2O (pH 7.4) HEPES buffer solution **(c)** Fluorescence spectra and **(d)** Absorption spectra of **HCFH** after addition of Cu^{2+} with different counter anions in H_2O (pH 7.4) HEPES buffer solution.

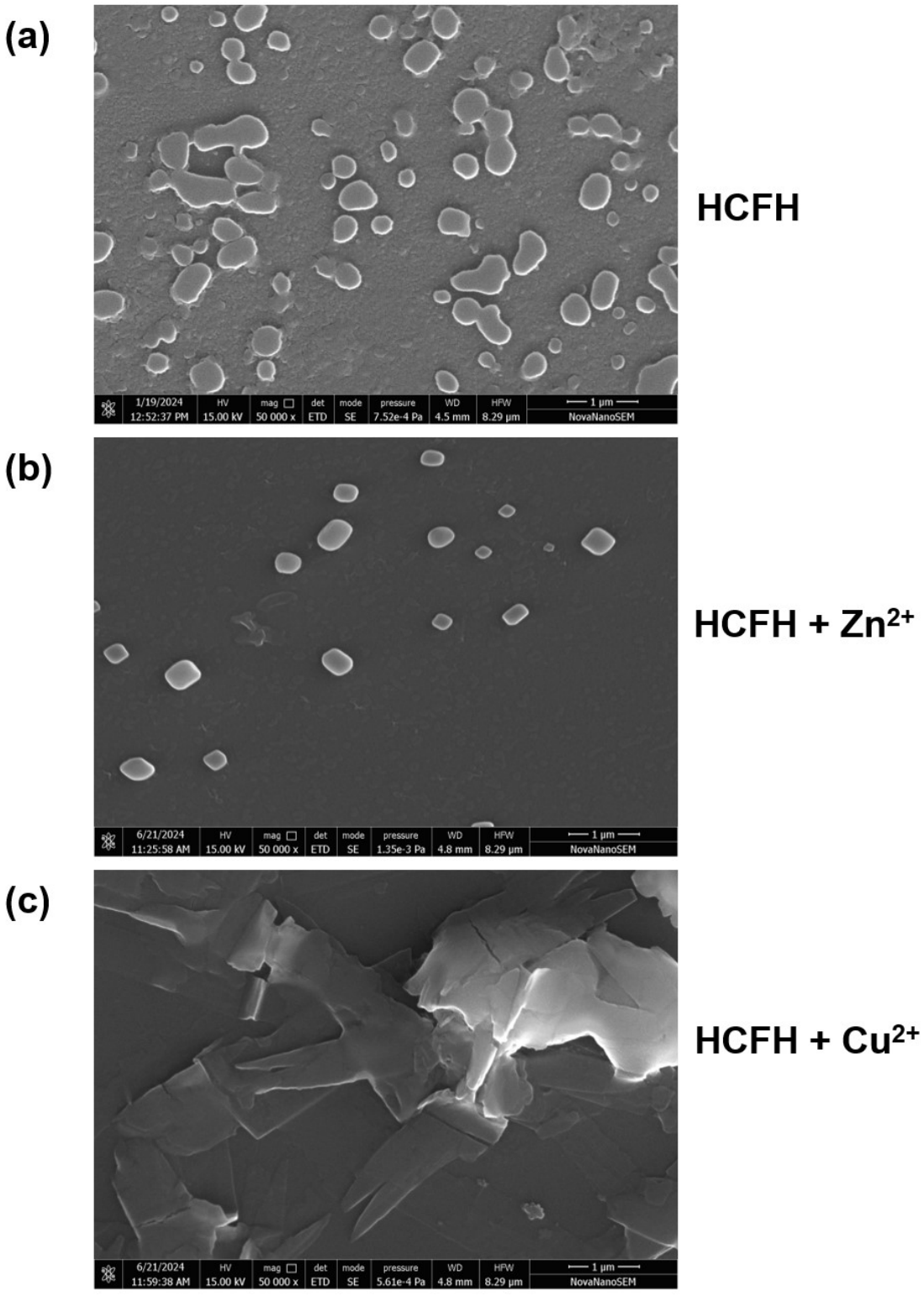

Fig. S14 (a) Surface morphology of **HCFH**, **(b)** Surface morphology of **HCFH** after the interaction with Zn^{2+} and **(c)** Surface morphology of **HCFH** after the interaction with Cu^{2+} (Scale 1µm).

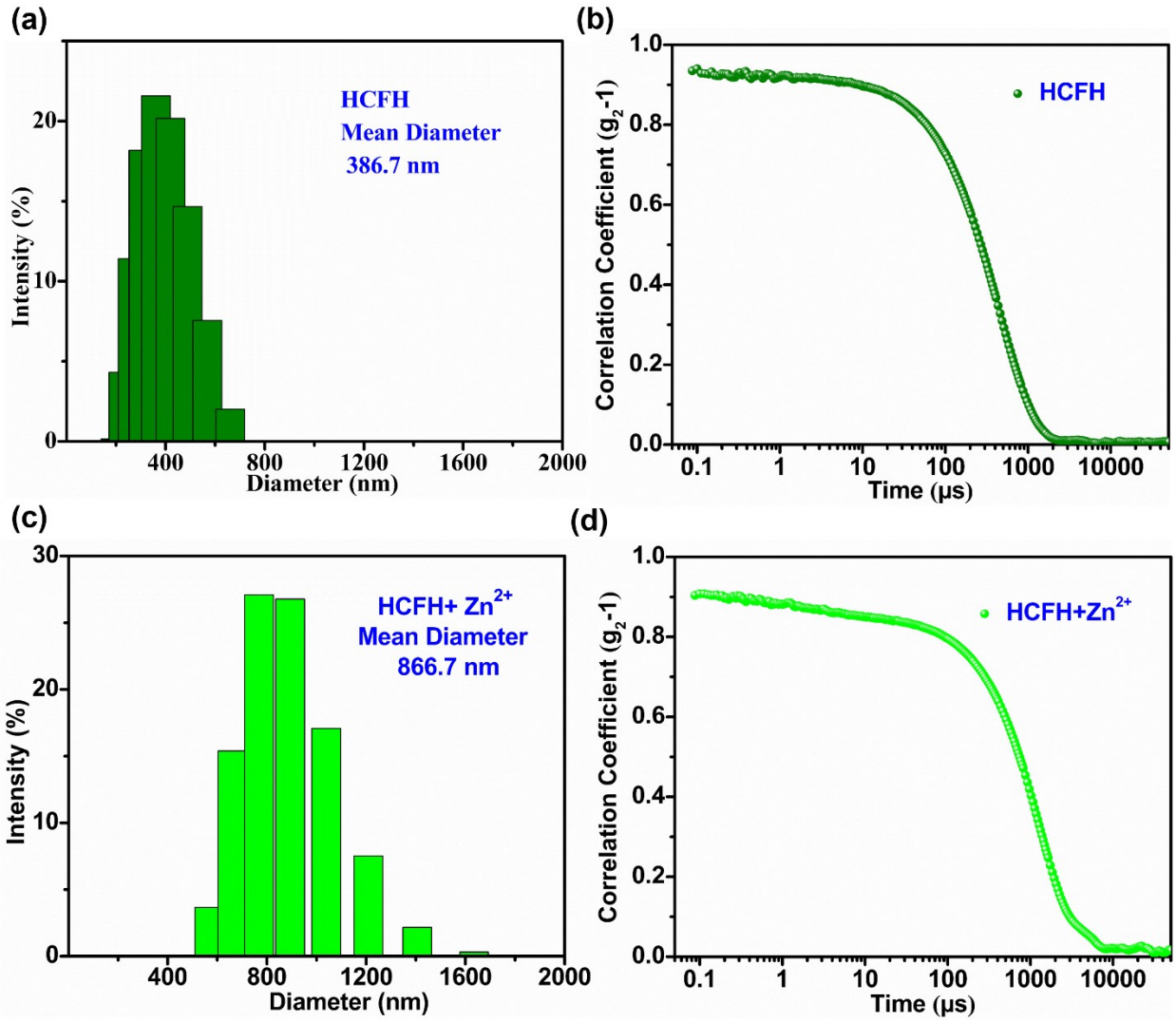

Fig. S15 (a) Particle size of **HCFH** (20 μM) measured with DLS in water **(b)** Correlation coefficient vs time profile diagram for **HCFH** (20 μM) measured with DLS in water **(c)** Particle size of **HCFH** + Zn^{2+} (20 μM) measured with DLS in water **(d)** Correlation coefficient vs time profile diagram for **HCFH** + Zn^{2+} (20 μM) measured with DLS in water.

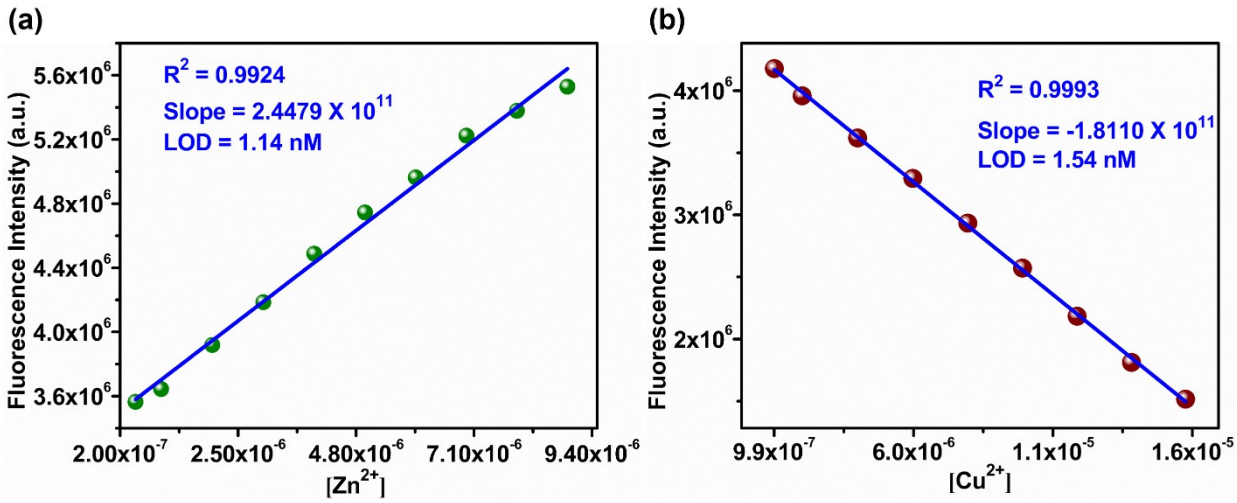

Fig. S16 Limit of detection (LOD = 3σ/Slope) curve plot, the change in fluorescence intensity at 496 nm of **HCFH** (20 μM) as a function of **(a)** Zn^{2+} concentration and **(b)** Cu^{2+} concentration.

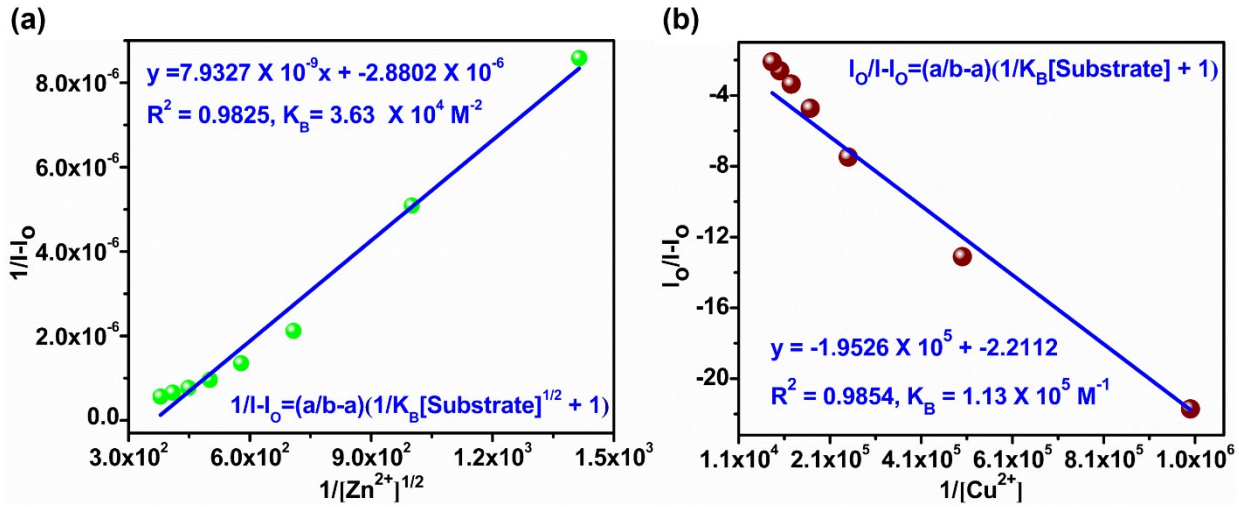

Fig. S17 Benesi-Hildebrand plot of **HCFH** for determination of binding constant with **(a)** Zn^{2+} and **(b)** Cu^{2+}. (R^2 denotes Goodness of fit). (λem = 496 nm, λex = 400 nm).

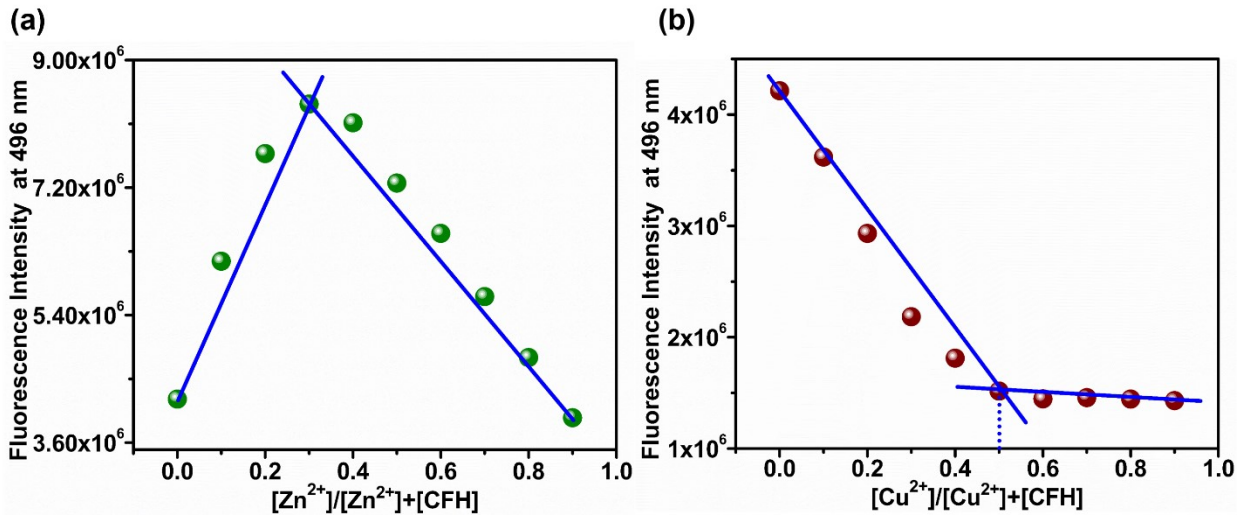

Fig. S18 (a) Job's plot for determination of binding stoichiometry of **HCFH**-Zn^{2+} and (b) binding stoichiometry of **HCFH**-Cu^{2+}.

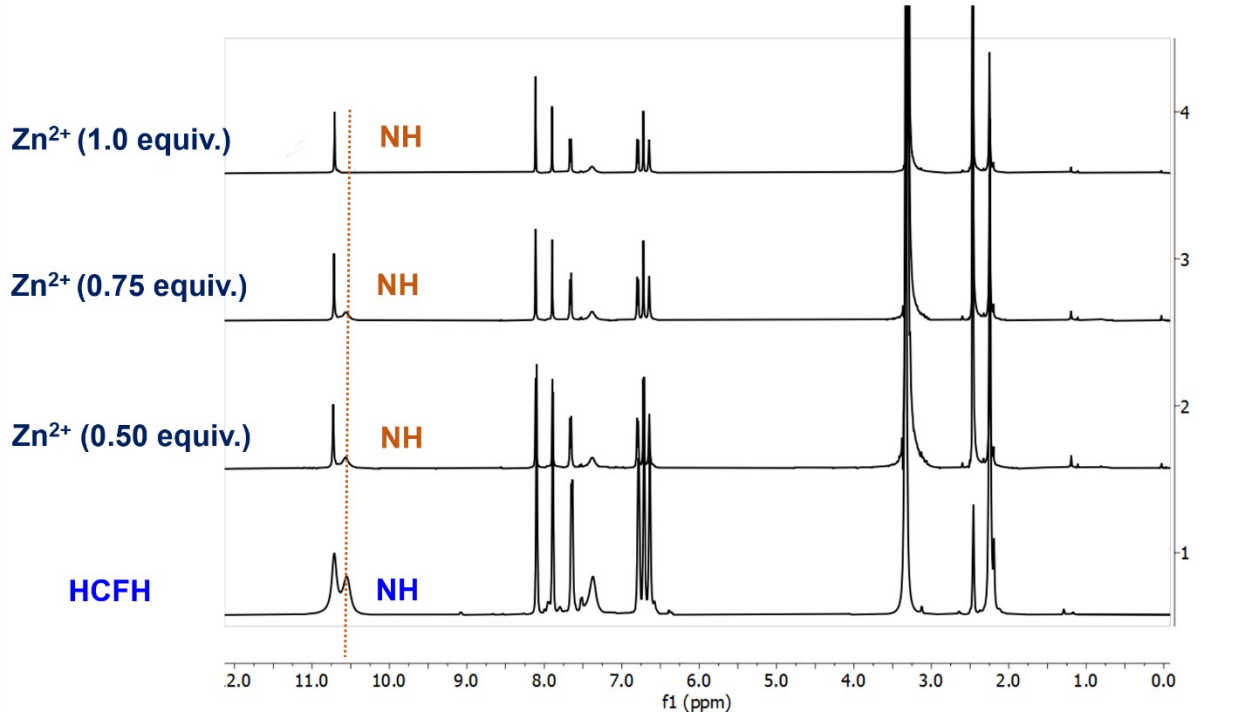

Fig. S19 ^1H NMR titration of **HCFH** after addition of Zn^{2+} (0-1 equiv.) in DMSO–d_6.

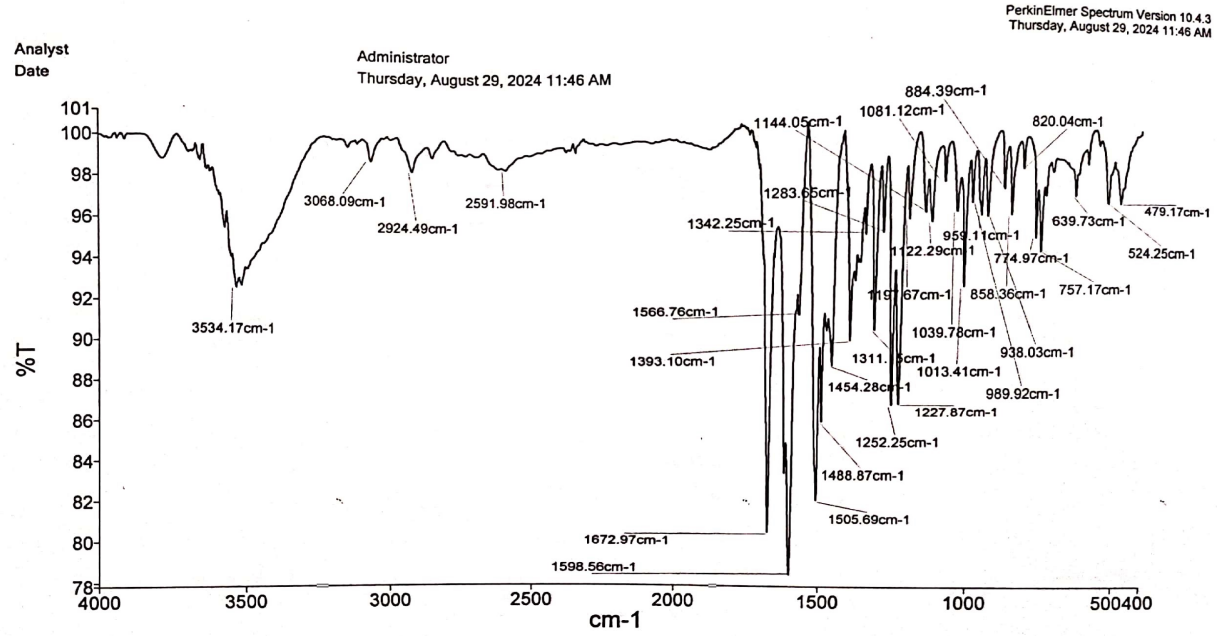

Fig. S20 IR spectrum of **HCFH**-Zn^{2+} complex.

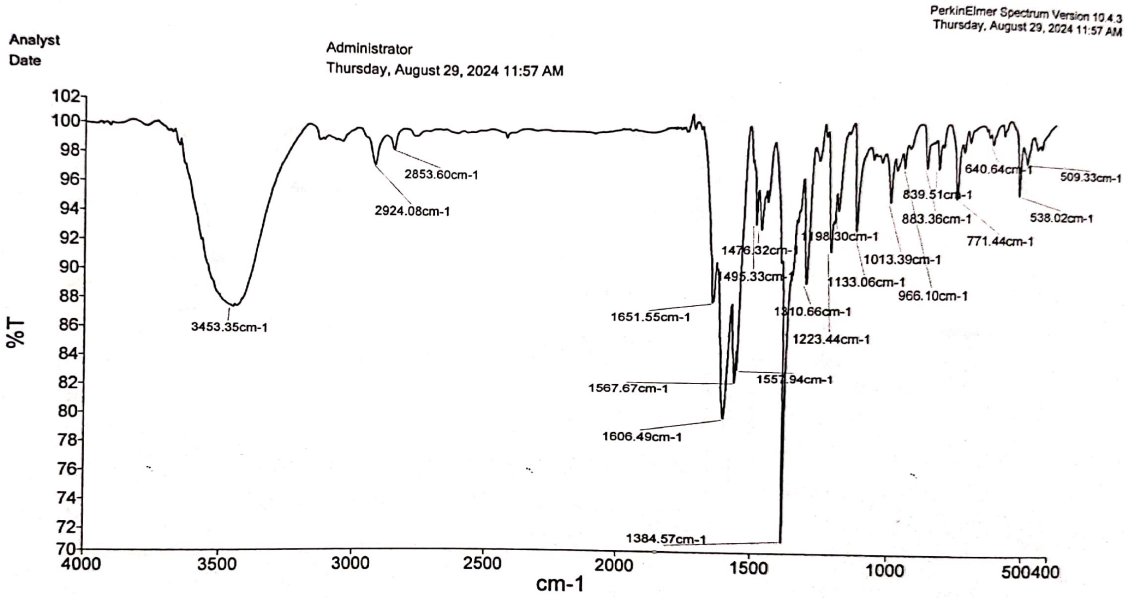

Fig. S21 IR spectrum of **HCFH**-Cu^{2+} complex.

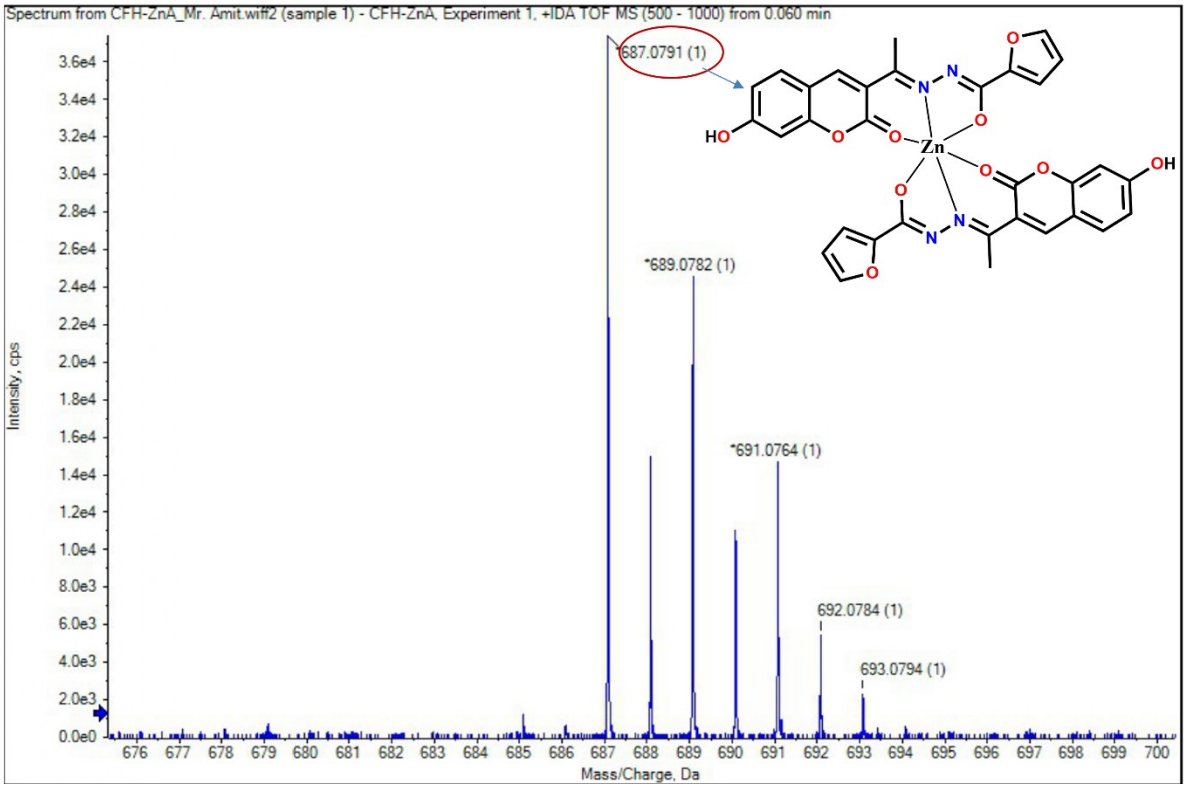

Fig. S22 Mass spectrum of **HCFH**-Zn^{2+} complex.

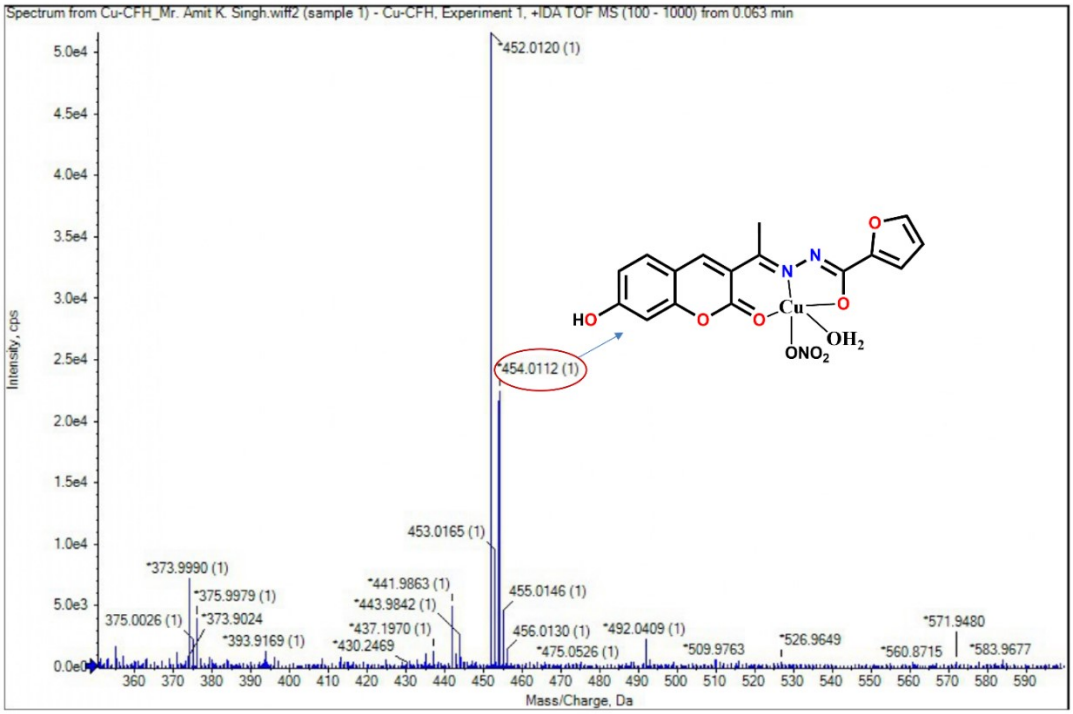

Fig. S23 Mass spectrum of **HCFH**-Cu^{2+} complex

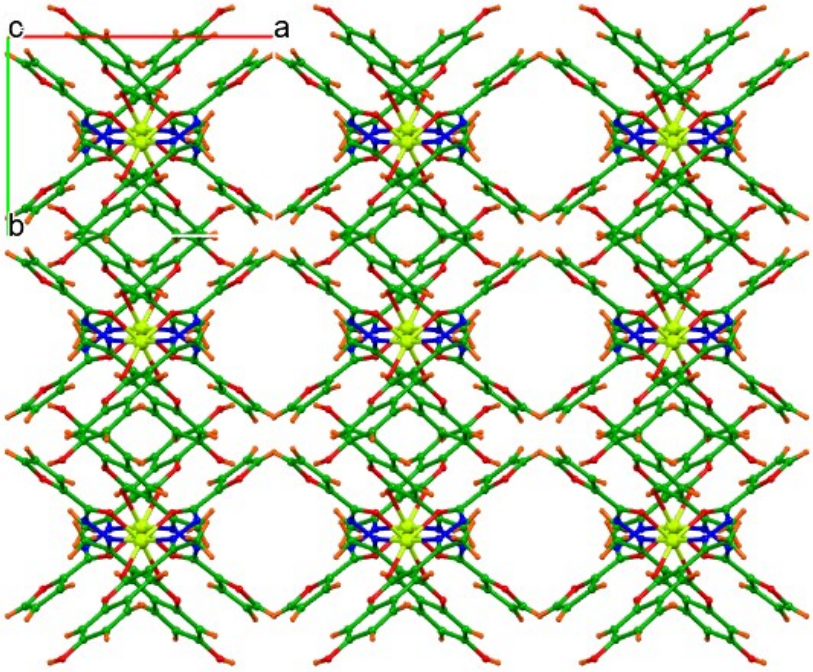

Fig. S24 Crystal packing structure of **HCFH**-Zn^{2+} complex and its molecular assembly.

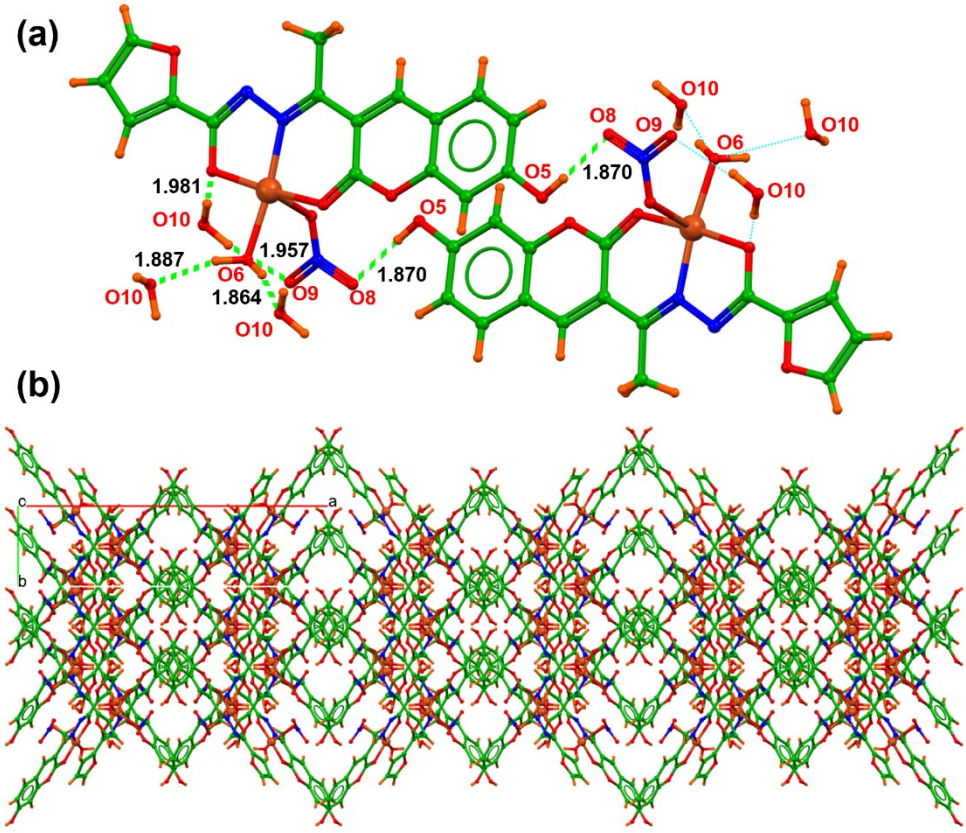

Fig. S25 Crystal packing structure of **HCFH**-Cu^{2+} complex and its molecular assembly.

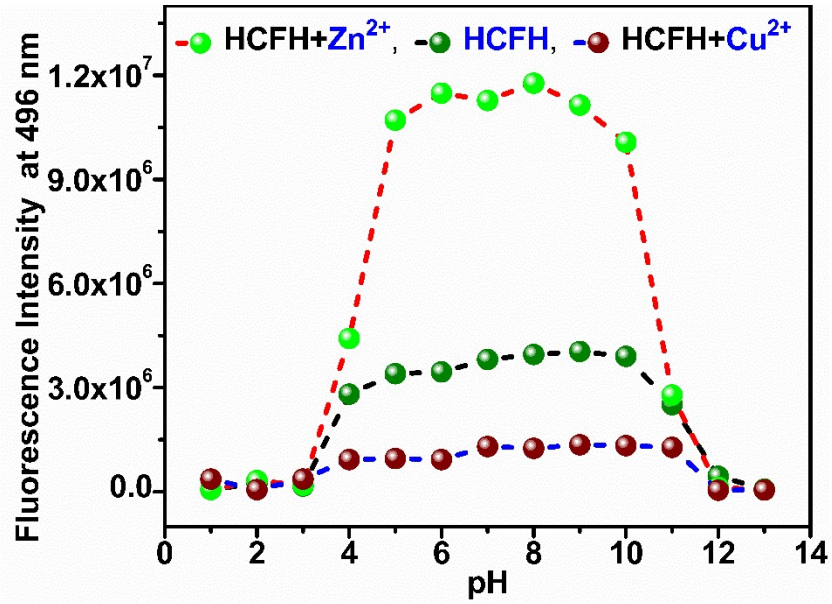

Fig. S26 Effect of pH variation on the fluorescence intensities of **HCFH** (20 μM) in H_2O (pH 7.4) HEPES buffer solution, and after addition of Zn^{2+} and Cu^{2+} (20 μM), (λ_{em} = 496 nm, λ_{ex} = 400 nm).

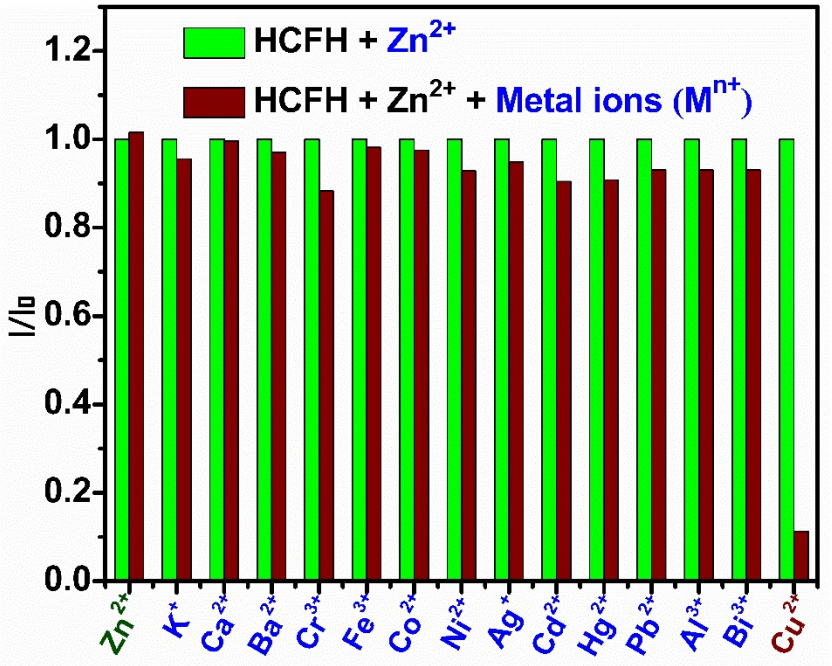

Fig. S27 Fluorescence intensity variation of **HCFH** (20 μM) in the presence of Zn^{2+} (20 μM) with addition of different metal ions (20 μM) in H_2O (pH 7.4, HEPES buffer solution), (λ_{em} = 496 nm, λ_{ex} = 400 nm).

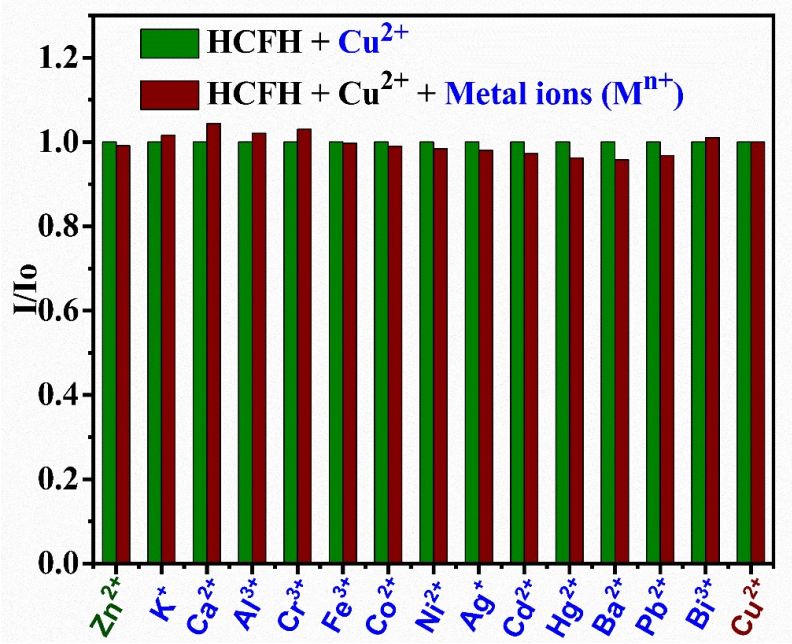

Fig. S28 Fluorescence intensity variation of **HCFH** (20 μM) in the presence of Cu^{2+} (20 μM) with addition of different metal ions (20 μM) in H_2O (pH 7.4, HEPES buffer solution). (λ_{em} = 496 nm, λ_{ex} = 400 nm).

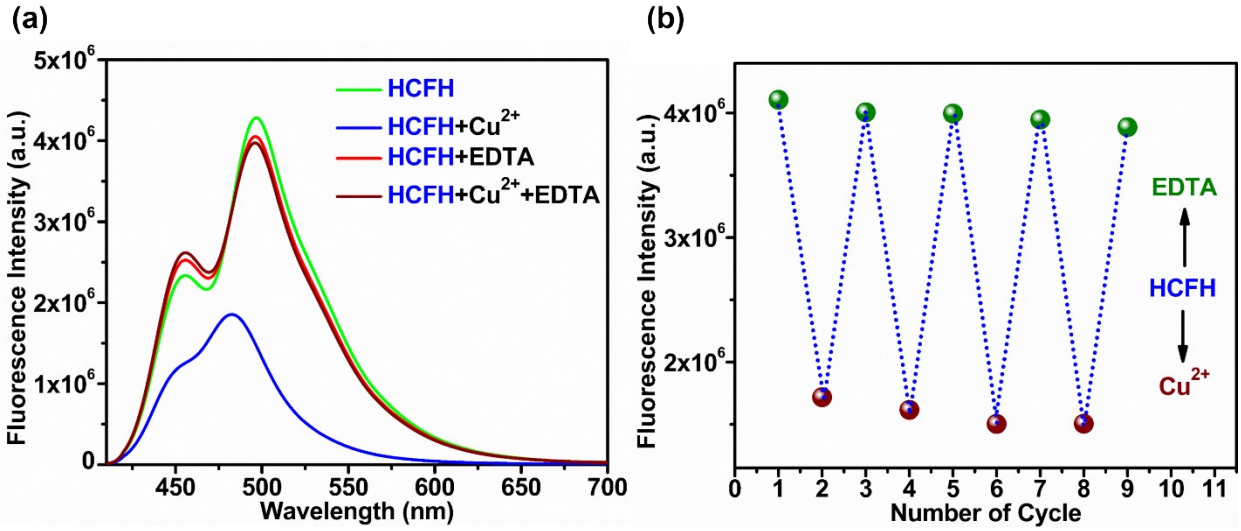

Fig. S29 (a) Fluorescence intensity of **HCFH** (20 μM) upon subsequent addition Cu^{2+} and EDTA, **(b)** Reversible performance of **HCFH** up to four cycles (at 496 nm).

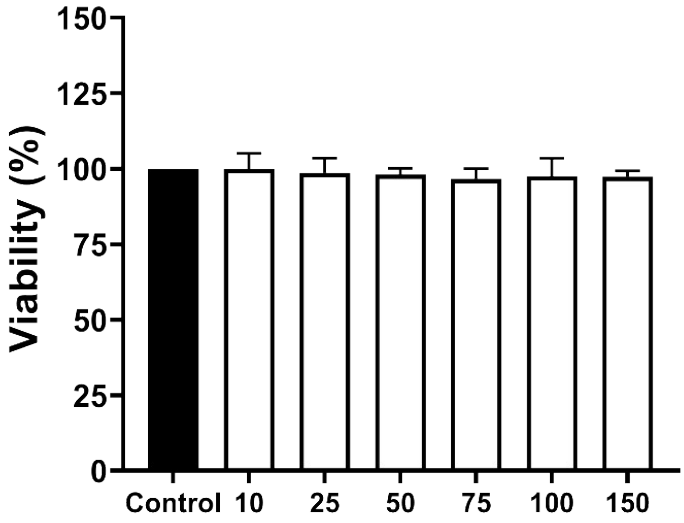

Fig. 30 MTT assay plot showing treatment of HeLa cells with various concentration of **HCFH** (10, 25, 50, 75, 100 and 150 μM) for 12 h.

Table S1 Crystallographic data for **HCFH**, **HCFH**-Zn^{2+} and **HCFH**-Cu^{2+}

Parameters	**HCFH**	**HCFH-Zn^{2+}**	**HCFH-Cu^{2+}**
CCDC	**2289442**	**2343626**	**2328887**
Empirical formula	$C_{16}H_{12}N_2O_5$	$C_{18}H_{18}N_2O_6SZn_{0.5}$	$C_{16}H_{15}CuN_3O_{10}$
Formula weight	312.28	423.09	493.01
Temperature/K	293	100.15	293
Crystal system	monoclinic	monoclinic	monoclinic
Space group	$P2_1/c$	P2/c	C2/c
a/Å	8.23546(5)	12.1405(7)	27.1875(9)
b/Å	23.11379(13)	8.8776(5)	6.49900(10)
c/Å	7.69661(5)	16.5239(12)	24.9525(6)
α/°	90	90	90
β/°	101.9965(6)	101.958(7)	112.195(4)
γ/°	90	90	90
Volume/$Å^3$	1433.074(15)	1742.27(19)	4082.2(2)
Z	4	4	8
ρ_{calc} g/cm^3	1.447	1.613	1.604
μ/mm^{-1}	0.925	2.736	2.056
F(000)	648.0	876.0	2088.0
Crystal size/mm^3	0.23 × 0.13 × 0.1	0.13 × 0.11 × 0.09	0.25 × 0.2 × 0.17
Radiation	Cu Kα (λ = 1.54184)	Cu Kα (λ = 1.54184)	Cu Kα (λ = 1.54184)
2Θ range for data collection/°	7.65 to 143.948	10.946 to 143.94	7.024 to 144.538
Index ranges	-10 ≤ h ≤ 10, -28 ≤ k ≤ 28, -9 ≤ l ≤ 8	-14 ≤ h ≤ 14, -10 ≤ k ≤ 10, -19 ≤ l ≤ 19	-33 ≤ h ≤ 33, -7 ≤ k ≤ 5, -30 ≤ l ≤ 30
Reflections collected	47078	15791	15546
Independent reflections	2820 [R_{int} = 0.0237, R_{sigma} = 0.0084]	3302 [R_{int} = 0.1038, R_{sigma} = 0.0935]	3921 [R_{int} = 0.0667, R_{sigma} = 0.0498]
Data/restraints/parameters	2820/0/216	3302/0/215	3921/0/277
Goodness-of-fit on F^2	1.099	1.060	1.115
Final R indexes [I>=2σ (I)]	R1 = 0.0349, wR2 = 0.1014	R1 = 0.1151, wR2 = 0.2613	R1 = 0.0801, wR2 = 0.2073
Final R indexes [all data]	R1 = 0.0365, wR2 = 0.1027	R1 = 0.1595, wR2 = 0.2877	R1 = 0.0876, wR2 = 0.2134
Largest diff. peak/hole / e $Å^{-3}$	0.17/-0.17	0.73/-0.46	1.27/-0.93

[a] $R_1 = \Sigma||F_o| - |Fc||\Sigma|F_o|$. [b] $R_2 = [\Sigma w(|F^2_o| - |F^2_c|)^2/\Sigma w|F^2_o|^2]^{1/2}$

Table S2 Bond lengths for **HCFH**

Bonds	Length/Å	Bonds	Length/Å
O4-C15	1.3750(14)	C10-O11	1.4013(17)
O4-C16	1.3739(15)	C8-C9	1.3453(18)
O1-C4	1.3618(16)	C8-C16	1.4564(18)
O1-C1	1.3630(16)	C8-C7	1.4870(16)
O5-C13	1.3531(14)	C14-C13	1.3826(17)
O2-C5	1.2196(16)	C11-C12	1.3692(18)
O3-C16	1.2038(16)	C13-C12	1.3946(18)
N2-N1	1.3799(14)	C5-C4	1.4611(17)
N2-C7	1.2771(16)	C4-C3	1.3386(19)
N1-C5	1.3494(17)	C7-C6	1.4967(19)
C15-C10	1.3943(16)	C3-C2	1.417(2)
C15-C14	1.3796(16)	C2-C1	1.325(2)
C10-C9	1.4281(16)		

Table S3 Bond angles for **HCFH**

Bonds	Angle/°	Bonds	Angle/°
O1-C1-C2	110.47(13)	O5-C13-C14	121.88(11)
C1-C2-C3	106.82(13)	C12-C11-C10	121.20(11)
C2-C3-C4	106.45(14)	C15-C14-C13	118.29(11)
C6-C7-C8	120.60(12)	C8-C9-C10	121.98(11)
C6-C7-N2	125.04(12)	C16-C8-C7	117.45(11)
C8-C7-N2	114.35(11)	C9-C8-C7	122.74(11)
C11-C12-C13	120.04(12)	C9-C8-C16	119.67(11)
C3-C4-C5	131.00(13)	C11-C10-C9	125.24(11)
C3-C4-O1	110.04(12)	C15-C10-C11	117.00(11)
O1-C4-C5	118.92(11)	C15-C10-C9	117.76(11)
O3-C16-C8	126.44(12)	C14-C15-C10	122.93(11)
O3-C16-O4	116.08(12)	O4-C15-C14	116.69(10)
O4-C16-C8	117.46(10)	O4-C15-C10	120.38(10)
N1-C5-C4	115.15(11)	C5-N1-N2	119.00(10)
O2-C5-C4	120.72(12)	C7-N2-N1	116.33(10)
O2-C5-N1	124.10(12)	C4-O1-C1	106.22(11)
C12-C13-C14	120.50(11)	C16-O4-C15	122.71(9)
C12-C13-O5	117.62(11)		

Table S4 Fluorescence decay parameters and quantum yields of **HCFH** in THF-H_2O (pH 7.4 HEPES buffer solution) mixtures at different fraction of water.

f_w	A	τ (ns)	<τ> (ns)	ϕ	K_r($^-$s)	K_{nr}($^-$s)
f_w=40%	0.098(A_1)	2.411(τ_1)	0.627	2.16 x 10^{-3}	3.44 x 10^6	1.58 x10^8
	0.855(A_2)	0.421(τ_2)				
f_w=80%	0.249(A_1)	2.173(τ_1)	1.250	4.18 x 10^{-3}	3.34 x 10^6	7.99 x 10^8
	0.602(A_2)	0.869(τ_2)				
f_w=99.99%	0.050(A_1)	2.411(τ_1)	0.780	2.01 x 10^{-3}	2.57 x 10^6	1.28 x 10^8
	0.805(A_2)	0.421(τ_2)				

Table S5 Fluorescence decay parameters and quantum yields of **HCFH** before and after treatment with Zn^{2+}/Cu^{2+} in H_2O (pH 7.4) HEPES buffer solution.

Sample	A	τ (ns)	<τ> (ns)	ϕ	K_r($^-$s)	K_{nr}($^-$s)
HCFH	0.047(A_1)	4.233(τ_1)	0.768	2.21 x 10^{-3}	2.87 x 10^6	1.29 x 10^8
	0.857(A_2)	0.576(τ_2)				
HCFH-Zn^{2+}	0.440(A_1)	1.174(τ_1)	2.011	6.19 x 10^{-3}	3.07 x 10^6	0.49 x 10^8
	0.403(A_2)	2.923(τ_2)				
HCFH-Cu^{2+}	0.841(A_1)	0.385(τ_1)	0.584	0.46 x 10^{-3}	0.78 x 10^6	1.71 x 10^8
	0.104(A_2)	2.195(τ_1)				

Table S6 Major bond lengths and bond angle for **HCFH**-Zn^{2+}.

Bonds	**Length/Å**	**Bonds**	**Angle/°**
Zn-O2	2.049(5)	O2-Zn- O2[1]	103.2(3)
Zn-O2[1]	2.049(5)	O2-Zn-O3	159.0(2)
Zn-O3	2.132(6)	O2- Zn-O3[1]	89.5(2)
Zn-O3[1]	2.132(6)	O2[1]-Zn-O3	89.5(2)
Zn-N2	2.112(6)	O2[1]-Zn-O3[1]	159.0(2)
Zn-N2[1]	2.112(6)	O2[1]-Zn-N2	98.6(2)
O2-C5	1.255(9)	O2-Zn- N2[1]	98.6(2)
O3-C16	1.999(9)	O2[1]-Zn-N2[1]	78.1(2)
N2-C7	1.297(10)	O2-Zn-N2	78.1(2)
N1-N2	1.399(8)	O3-Zn-O3[1]	83.7(3)
N1-C5	1.313(9)	N2[1]-Zn-O3[1]	83.6(2)
C6-C7	1.512(10)	N2-Zn-O3	83.6(2)
C7-C8	1.470(11)	N2[1]-Zn-O3	100.3(2)
C8-C16	1.470(11)	N2-Zn-O3[1]	100.3(2)
O4-C16	1.395(10)	N2-Zn-N2	174.8(3)

Table S7 Major bond lengths and bond angle for **HCFH**-Cu^{2+}.

Bonds	**Length/Å**	**Bonds**	**Angle/°**
Cu-O2	1.918(3)	O2-Cu-O3	173.35(13)
Cu-O3	1.927(3)	O2-Cu-O6	93.41(13)
Cu-O6	1.948(3)	O2-Cu-N2	83.39(13)
Cu-N2	1.939(3)	O3-Cu-O6	90.22(12)
Cu-O7	2.480(4)	O3-Cu-N2	92.36(13)
O2-C5	1.306(5)	N2-Cu-O6	172.77(14)
O3-C16	1.243(5)	O2-Cu-O7	88.8(1)
N2-C7	1.278(5)	O3-Cu-O7	97(1)
N1-N2	1.405(5)	N2-Cu-O7	100.2(1)
N1-C5	1.306(5)	O6-Cu-O7	86.15(11)

Table S8 Comparison of **HCFH** with other previously reported sensors.

S. N.	Photophysical properties			Sensing			Biological applications	Miscellaneous	Ref.
	AIE	Viscoch romism	Piezoch romism	Sensing media	Analyte	Detection limit (M)			
1	✓	✓	✓	H_2O	Zn^{2+}, Cu^{2+}	Zn^{2+}: 1.14×10^{-9} Cu^{2+}: 1.54×10^{-9}	Live cell imaging, Mitotracking	Reversibility, Logic gates, Paper strip,	This work
2	×	×	×	CH_3CN:DMSO (9:1, v/v)	Zn^{2+}	Zn^{2+}: 1.79×10^{-6}	Live cell imaging	Reversibility, Logic gates	9
3	✓	✓	✓	DMF:H_2O (3:7, v/v)	Zn^{2+}, Cu^{2+}	Zn^{2+}: 2.97×10^{-9} Cu^{2+}: 6.75×10^{-9}	Live cell imaging	Reversibility, Logic gates	10
4	✓	×	×	DMF:H_2O (9:1, v/v)	Zn^{2+}	Zn^{2+}: 1.1×10^{-7}	N/A	Paper strip	11
5	✓	×	×	THF:H_2O (1:1, v/v)	Zn^{2+}, Cu^{2+}	Zn^{2+}: 1.3×10^{-8} Cu^{2+}: 1.6×10^{-6}	N/A	Real sample analysis	12
6	×	×	×	CH_3CN/H_2O (1:1, v/v)	Zn^{2+}	Zn^{2+}: 3.8×10^{-8} Cu^{2+}: 5.8×10^{-7}	N/A	Logic gates	13
7	✓	×	✓	MeOH:H_2O (1:1, v/v)	Zn^{2+}, Cu^{2+}	Zn^{2+}: 7.19×10^{-8} Cu^{2+}: 2.12×10^{-7}	N/A	N/A	14

References

1 S. Lee, K. Sivakumar, W.-S. Shin, F. Xie and Q. Wang, Synthesis and anti-angiogenesis activity of coumarin derivatives, *Bioorg. Med. Chem. Lett*, 2006, **16**, 4596–4599.

2 A. D. Becke, Density-functional thermochemistry. I. The effect of the exchange-only gradient correction, *J. Chem. Phys*, 1992, **96**, 2155–2160.

3 S. Yoshioka, Y. Inokuma, M. Hoshino, T. Sato and M. Fujita, Absolute structure determination of compounds with axial and planar chirality using the crystalline sponge method, *Chem. Sci.*, 2015, **6**, 3765–3768.

4 L. J. Farrugia, WinGX and ORTEP for Windows: an update. *J. Appl. Crystallogr.* 2012, **45**, 849–854.

5 P. Yadav, A. K. Singh, C. Upadhyay and V. P. Singh, Photoluminescence behaviour of a stimuli responsive Schiff base: Aggregation induced emission and piezochromism, *Dyes and Pigments*, 2019, **160**, 731–739.

6 K. R. Barqawi, Z. Murtaza and T. J. Meyer, Calculation of relative nonradiative decay rate constants from emission spectral profiles: polypyridyl complexes of ruthenium (II), *J. Phys. Chem*, 1991, **95**, 47–50.

7 G. L. Long and J. D. Winefordner, Limit of detection. A closer look at the IUPAC definition, *Anal. Chem*, 1983, **55**, 712A-724A.

8 H. A. Benesi and J. H. Hildebrand, A Spectrophotometric Investigation of the Interaction of Iodine with Aromatic Hydrocarbons, *J. Am. Chem. Soc*, 1949, **71**, 2703–2707.

9 A. K. R. Ahmed, R. Gajendhiran, S. Mithra, S. A. Majeed, A. S. S. Hameed, R. Paulpandiyan, S. Maniyammai, G. T. Senthil Andavan, M. NizamMohideen and A. K. Rahiman, Salicylidene-based dual-responsive 'turn on' fluorometric chemosensors for the selective detection of Zn^{2+}, Al^{3+} and F^{-} ions: theoretical investigation and applications in the live cell imaging of zebrafish larvae and molecular logic gate operation, *J. Mater. Chem. B*, 2025, **13**, 622–641.

10 A. Singh, P. Yadav, S. Singh, P. Kumar, S. Srikrishna and V. P. Singh, A multifunctional coumarin-based probe for distinguishable detection of Cu^{2+} and Zn^{2+}: its piezochromic, viscochromic and AIE behavior with real sample analysis and bio-imaging applications, *J. Mater. Chem. C*, 2023, **11**, 13056–13066.

11 M. Shyamal, P. Mazumdar, S. Maity, S. Samanta, G. P. Sahoo and A. Misra, Highly Selective Turn-On Fluorogenic Chemosensor for Robust Quantification of Zn (II) Based on Aggregation Induced Emission Enhancement Feature, *ACS Sens*, 2016, **1**, 739–747.

12 Q. Niu, T. Sun, T. Li, Z. Guo and H. Pang, highly sensitive and selective colorimetric/fluorescent probe with aggregation induced emission characteristics for multiple targets of copper, zinc and cyanide ions sensing and its practical application in water and food samples, *Sens. Actuators B Chem*, 2018, **266**, 730–743.

13 G. Gangatharan Vinoth Kumar, A. Awasthi and A. Draksharapu, Dual function Schiff-base as a selective fluorescence "Turn-on" sensor for Zn^{2+} and a colorimetric sensor for Cu^{2+} and Fe^{3+} ions, *J. Photochem. Photobio. A. Chem*, 2024, **454**, 115739.

14 M. Yang, Y. Zhang, W. Zhu, H. Wang, J. Huang, L. Cheng, H. Zhou, J. Wu and Y. Tian, Difunctional chemosensor for Cu(ii) and Zn(ii) based on Schiff base modified anthryl derivative with aggregation-induced emission enhancement and piezochromic characteristics, *J. Mater. Chem. C*, 2015, **3**, 1994–2002.